PHILOSOPHICAL MAGAZINE, 2003, VOL. 83, NO. 10, 1255–1286

On the calculation of the magnetoresistance of tunnel junctions with parallel paths of conduction

KUISING WANG†, PETER M. LEVY†, SHUFENG ZHANG‡, and LASZLO SZUNYOGH§ ||

† Department of Physics, New York University, 4 Washington Place, New York, New York 10003, USA
‡ Department of Physics and Astronomy, University of Missouri, Columbia, Missouri 65211, USA
§ Department of Theoretical Physics, Budapest University for Technology and Economics, Budafokiút 8, 1521 Budapest, Hungary
|| Institut für Technische Electrochemie, Technische Universität Wien, A-1060 Wien, Austria

[*Received 27 October 2002 and accepted 31 October 2002*]

ABSTRACT

At the interfaces between the metallic electrodes and barrier in magnetic tunnel junctions it is possible for localized states to form which are orthogonal to the itinerant states for the junction, as well as resonant states that can form at the interfaces. These states form highly conducting paths across the barrier when their orbitals point directly into the barrier; these paths are in addition to those formed by the itinerant states across the entire junction. Most calculations of transport in magnetic tunnel junctions are made with the assumptions that the transverse momentum of the tunnelling electrons is conserved, in which case the itinerant electron states remain orthogonal to localized states. In principle it is possible to include diffuse scattering in both the bulk of the electrodes and the barrier so that the transverse momentum is not conserved, as well as the processes that couple localized states at the electrode–barrier interface to the itinerant states in the bulk of the electrodes. However, including these effects leads to lengthy calculations. Therefore, to assess the conduction across the barrier through the localized states that exist in parallel to the itinerant states we propose an approximate scheme in which we calculate the conductance of only the barrier region. While we do not take explicit account of either of the effects mentioned above, we do calculate the tunnelling through all the states that exist at the electrode–barrier interfaces by placing reservoirs directly across the barriers. To calculate the current and magnetoresistance for magnetic tunnel junctions (the junction magnetoresistance (JMR)) we have used the lattice model developed by Caroli *et al*. The propagators, density of states and hopping integrals entering the expressions for the current are determined by using the spin polarized scalar-relativistic screened Korringa–Kohn–Rostoker method that has been adapted to layered structures. By using vacuum as the insulating barrier we have determined with no adjustable parameters the JMR in the linear response region of tunnel junctions with fcc Co(100), fccNi(100) and bcc Fe(100) as electrodes. The JMR ratios that we find for these metal/vacuum/metal junctions are comparable with those measured with alumina as the insulating barrier. For vacuum barriers we find that tunnelling currents have minority-spin polarization whereas the tunnelling currents for these electrodes have been observed to be positively (majority) polarized for alumina barriers and minority polarized for $SrTiO_3$ barriers. In addition to determining the JMR ratios in linear

Philosophical Magazine ISSN 1478–6435 print/ISSN 1478–6443 online © 2003 Taylor & Francis Ltd
http://www.tandf.co.uk/journals
DOI: 10.1080/0141861031000065077

response we have also determined how the magnetoresistance of magnetic tunnel junctions varies with a finite voltage bias applied across the junction. In particular we have found how the shape of the potential barrier is altered by the applied bias and how this affects the current. Comparisons with data as they become available will eventually determine whether our approximate scheme or the ballistic Landauer–Büttiker approach is better able to represent the features of the electronic structure that control tunnelling in magnetic tunnel junctions.

§ 1. Introduction

The junction magnetoresistance (JMR) refers to the fact that in a magnetic tunnel junction (MTJ), that is ferromagnetic metal/insulator/ferromagnetic metal junction, the current depends on the relative orientation of the magnetizations of the two electrodes. Usually a larger current is observed when the magnetizations are parallel than when they are antiparallel (Julliere 1975, Maekawa and Gäfvert 1982), although recently an inverse JMR has been observed for which the current for the antiparallel configuration of the magnetic electrodes is larger (De Teresa *et al.* 1999a,b). Theoretical explanations of the JMR have been mainly based on the transfer Hamiltonian approach (Duke 1969, Maekawa and Gäfvert 1982, Meservey and Tedrow 1994, Inoue and Maekawa 1996). Recently there has been much interest in interpreting experimental results in terms of realistic band structures. Butler *et al.* (1997, 2001) and MacLaren *et al.* (1997, 1999) based their calculations on the Landauer (1988)–Büttiker (1988) (LB) formula. Starting from bulk metal hopping integrals, Mathon (1997) and Mathan and Umerski (2001) discussed changes in JMR with coupling strength in terms of a tight-binding version of the Kubo–Greenwood formula by artificially cleaving the bulk Co metal into two separate parts and then joining them up with hopping integrals while Tsymbal and Pettifer (1997) studied the spin polarization of tunnelling from Co and Ni by modelling the insulator as simply a gap in the band structure and the electrodes as if they had a single band. To understand the origin of the majority spin polarization of tunnelling currents observed across alumina barriers, Oleinik *et al.* (2000) have undertaken a calculation of the density of states (DOS) inside the barrier, while Tsymbal *et al.* (2000) studied the influence of an oxide monolayer on the surface DOS of Fe.

When one thinks of conduction across a tunnel junction the first thing that comes to mind is the transmission from the states deep in one electrode to those of the other electrode, that is conduction across the itinerant states of the entire junction. At the interfaces between the electrodes and the tunnelling barrier, localized states form which can have orbitals that project into the tunnelling barrier and thereby form another bridge for conduction across the barrier, that is a parallel path for conduction. These localized states are in addition to the resonant states (Butler *et al.* 1997, 2001, MacLaren *et al.* 1997, 1999) that couple to the itinerant states at the interfaces; the itinerant states avoid the localized states and are orthogonal to them as long as there is no scattering in the junction other than that coming from the 'perfect' interfaces. Underlying the ballistic approach, as it has been applied to tunnelling in MTJs, that is conserving momentum in the plane of the layers $\mathbf{k}_{\|}$, is the assumption that the transport across the whole junction is coherent, that is no scattering other than the specular scattering at perfect interfaces. In this limit, conduction across the junction is limited to the itinerant states spanning the entire

junction. However, in the MTJs studied to date the diffuse scattering at the interfaces between the electrodes and the barrier and within the electrodes affect tunnelling; among other things it couples the two conduction paths (Pendry *et al*. 1991, Levy *et al*. 2002). In principle it is possible to take account of these additional processes to tunnelling conduction; indeed this was achieved by using a single orbital 1s tight-binding description for disordered wires by Todorov (1996). However, the *ab initio* calculations made to date are sufficiently difficult without these added complications so that their contributions have not been considered. To determine the amount of conduction that can take place through the parallel conduction path arising from localized states we calculate the transport *solely for the barrier region* of the junction; this is achieved by placing reservoirs directly across the interfaces of the junction. In this way all the states at the electrode–barrier interfaces, localized as well as itinerant, contribute to tunnelling; thereby we accent the role of the interfacial DOS in controlling tunnelling. Among other things, this approach circumvents the putative problem of how states that are localized at the interfaces contribute to tunnelling when they are orthogonal to the itinerant states in the electrodes for a perfect junction which has only specular scattering. In this paper we compare the $\mathbf{k}_{\|}$-resolved DOS and tunnelling currents for model MTJs with vacuum barriers found with our scheme, that is across the barrier alone, to those in the traditional LB approach as it has been applied to MTJs in which one does not take account of diffuse scattering or localized states. Comparisons with data as they become available will eventually determine whether our approximation or the ballistic ($\mathbf{k}_{\|}$-conserved) LB approach is better able to represent the features of the electronic structure that control tunnelling in MTJs.

As we are placing reservoirs directly across the barrier, that is in regions where there is scattering, we cannot use the Landauer formalism *per se*, because one must be in the asymptotic region outside the scattering region to define a transmission matrix. Therefore as we explain in the next section we have adapted another method introduced by Caroli *et al*. (1971) which defines the transport properties in terms of $\mathbf{t}$ matrices and concomitantly is not restricted to placing reservoirs in scattering free regions. Here we describe a calculation of the tunnelling current for bcc Fe(100)/vacuum/Fe(100), for fcc Co(100)/vacuum/Co(100) and fcc Ni(100)/vacuum/Ni(100) junctions for both parallel and antiparallel alignments of the magnetic moments of the electrodes. The tunnelling conductance and JMR of the barrier region are calculated by adapting a tight-binding version of the formula given by Todorov *et al*. (1993) as discussed in the next section. We obtain *ab initio* band structures from the spin polarized scalar-relativistic Screened Korringa–Kohn-Rostoker (SKKR) method as it has been adapted for layered structures, and s, p and d electrons are considered (Szunyogh *et al*. 1996, Wang 1999) and in § 3 we derive the relation between the tight-binding description in which the conductance is written and the SKKR method. In § 4 we present the results of these calculations, and in § 5 we discuss the conduction in the tunnel junction as taking place through two independent paths of conduction.

The effect of an external field on a metal surface is by and of itself an interesting subject; for example, it enters one's interpretation of scanning tunnelling microscopy (STM) data (Papanikolaou *et al*. 2000, Wortmann *et al*. 2001). In this paper we look at this in the context of the effect of an applied voltage bias on the magnetotransport properties of a MTJ. As most calculations of the JMR are currently limited to the linear response region, in this paper we push our

effort one step further by introducing a finite voltage bias into the calculation of the JMR. In particular we shall address the bias dependence of the tunnelling current and JMR. One of the major obstacles when making 'open circuit' transport calculations between two electrodes with different Fermi energies, that is for a tunnel junction that is not part of a closed circuit, is that self-consistency mandates that under an applied voltage there is a redistribution of electrons between electrodes so as to re-equilibrate the Fermi levels in both electrodes. However, what actually transpires in a junction that is part of a closed circuit and maintains a potential drop across it in the presence of a current is that the electron loss (gain) from an electrode is replenished (removed) by the wire completing the circuit. As we show in § 6, we are able to mimic the effects of voltage on the junction without undoing the difference in the electrode Fermi levels. In the last section we present our conclusions.

§ 2. The tight-binding model of tunnelling

As shown by Caroli *et al.* (1971, 1972), Combescot (1971) and Todorov *et al.* (1993) in the presence of an external voltage W, the net tunnelling current density (current per 2D atomic area) across a tunnelling junction is

$$j = \frac{2\pi e}{\hbar} \int_{\mu}^{\mu+eW} \mathrm{d}\varepsilon \, \mathrm{Tr}\,[\rho^{\alpha}(\varepsilon)[t^{\dagger}]^{\alpha\beta}(\varepsilon)\rho^{\beta}(\varepsilon)t^{\beta\alpha}(\varepsilon)], \tag{1}$$

where μ and $\mu + eW$ are the Fermi levels of the left- and right-hand electrodes respectively. In the linear response region, the tunnelling conductance reduces to

$$\mathbf{G} = \frac{j}{W} = \frac{2\pi e^2}{\hbar} \mathrm{Tr}\,[\rho^{\alpha}(\epsilon_{\mathrm{F}})[t^{\dagger}]^{\alpha\beta}(\epsilon_{\mathrm{F}})\rho^{\beta}(\epsilon_{\mathrm{F}})t^{\beta\alpha}(\epsilon_{\mathrm{F}})]. \tag{2}$$

In these expressions $t^{\alpha\beta}$ is the **t** matrix between two planes (layers) in the junction, and ρ^{α} and ρ^{β} are the density of states at the Fermi level. In real junctions,

(i) there is diffuse scattering in the electrodes,
(ii) the band bottoms of the electrodes are not flat in the vicinity of the barrier owing to charge transfer between the metallic electrodes and the insulating barrier and
(iii) localized states form at the electrode–barrier interfaces.

To account properly for these effects on the tunnelling current density is quite difficult in an *ab initio* calculation; therefore we have opted for an approach in which we calculate the conductance of a *part of* the junction. That is, we propose to calculate the conductance only across the barrier region by taking the **t** matrix $t^{\alpha\beta}$, where α and β are the electrode layers adjacent to the barrier; therefore the physical conductor that we consider is different from that in the two-terminal Landauer approach for the entire tunnel junction. In this approach we do not consider the resistance of the electrodes at all but, from experimental data on MTJs one knows that this is not a serious omission. Also we sidestep the problem of how the localized states communicate with the itinerant current-carrying states in the electrodes; by placing reservoirs across the layers containing these localized states (which is what one does to specify the voltage drop across two layers) and thereby filling them as they are depleted when they conduct, these participate in tunnelling conduction. The latter implies that the localized states remain in equilibrium with those

of the electrodes†, and we have justified this assumption elsewhere (Levy *et al*. 2002). In other words, we are saying that it *may* be a better approximation to calculate the resistance of a tunnelling junction solely across its barrier, by using equation (2) and identifying α and β as the electrode layers that are adjacent to the barrier, than to carry out a ballistic calculation of the entire junction in which one overlooks the possible contribution of a parallel path of conduction through localized states at the interfaces (Levy *et al*. 2002).

There are two steps in the scheme that we employ to calculate the transport in a tunnel junction. In the first step we calculate the electronic structure and obtain the full Green's functions and **t** matrices for the actual MTJ. In this phase there are no approximations. In the second step we make a ballistic calculation on an artificial system, the barrier butt up against reservoirs. In other words while we made a self-consistent determination of the layerwise electronic structure in the *entire* MTJ in the first step, in the second step when it comes to calculating the conductance we consider *only* the barrier region. In this manner we are assured that the states at the electrode–barrier interface are filled with electrons up to the Fermi level; this would not be the case in a ballistic calculation, $\mathbf{k}_{\|}$ conserved, across the *entire* junction. We stress that we do not perform a calculation that includes diffusive processes; rather we suggest that our approach, of placing reservoirs at the interfaces, simulates these processes inasmuch as we fill states that would not be filled in a ballistic calculation for the entire junction. While we introduce this method as a proposition, and not a proof, that one produces the correct conductance, there is nonetheless support for it. Datta (1995) has shown that by starting with the transfer Hamiltonian formalism, one can write the conductance of a conductor as we propose to do.

To summarize our approach, the conductor that we consider is different from the physical conductor. In our approach we sidestep the problem of how the localized states communicate with the itinerant current-carrying states in the electrodes; by placing reservoirs across the barrier region which contain these localized states (which is what one does to specify the voltage) and thereby filling them as they are depleted when they conduct, they participate in tunnelling conduction. In other words, we are saying that it *may* be a better approximation to calculate the resistance of just the barrier region than to carry out a ballistic calculation of the physical junction in which one overlooks the diffuse scattering and the possible contribution of localized states (Levy *et al*. 2002, Wunnicke *et al*. 2002).

The **t** matrix is defined in terms of the propagator **G** for the junction:

$$\mathbf{t} = \mathbf{V} + \mathbf{VGV}, \tag{3}$$

where, in a tight-binding description in which we assume that hopping occurs across neighbouring planes, **V** represents in the context of our calculation the hopping between the electrodes and the barrier at their interfaces:

$$\begin{aligned} V^{ij} &= \langle i|\mathbf{V}|j\rangle \\ &= V^{\alpha a}\delta^{i\alpha}\delta^{ja} + V^{a\alpha}\delta^{ia}\delta^{j\alpha} + V^{\beta b}\delta^{i\beta}\delta^{jb} + V^{b\beta}\delta^{ib}\delta^{j\beta}. \end{aligned}$$

† We acknowledge with thanks several discussions with professor Supriyo Datta. In particular he suggested the concept of parallel paths of conduction and brought up the question of maintaining the localized states in equilibrium in the presence of a current.

From the definition of **t**,

$$\begin{aligned}\langle i|\mathbf{t}|j\rangle &= t^{\beta\alpha}\delta^{i\beta}\delta^{j\alpha} + t^{\alpha\beta}\delta^{i\alpha}\delta^{j\beta} \\ &= V^{\beta b}G^{ba}V^{a\alpha}\delta^{i\beta}\delta^{j\alpha} + V^{a}G^{ab}V^{b\beta}\delta^{i\alpha}\delta^{j\beta}.\end{aligned} \tag{4}$$

Parenthetically, this allows us to interpret the transfer matrix $t^{\beta\alpha}$ as the product of the bonding of, or hopping from, the last layer of the right hand electrode, $V^{\beta b}$, on to the first layer of the insulating barrier, the propagation across the barrier, G^{ba}, and the bonding of the left-hand side of the barrier to the left-hand electrode, $V^{a\alpha}$. The coupling to more distant neighbouring planes is taken into account by using the principal layer description (Szunyogh *et al.* 1994). The DOSs are defined in terms of the Green's functions $\mathbf{g}(\epsilon)$ for the isolated (semi-infinite) electrodes

$$\boldsymbol{\rho}(\epsilon) = \frac{\mathbf{g}^{\dagger}(\epsilon) - \mathbf{g}(\epsilon)}{2\pi\mathrm{i}}. \tag{5}$$

These are different from the surface or bulk DOS inasmuch as the surface includes the transfer of the surface charge into the barrier (vacuum), and the bulk DOS contains hopping to the layers omitted in the definition of $\mathbf{g}(\epsilon)$ (Caroli *et al.* 1971, Toderov *et al.* 1993). While the transport is formulated in a tight-binding description we do *not* make the tight-binding parametrization; rather we obtain the hopping integrals from our *ab initio* calculations as described below.

For perfectly flat interfaces, translational symmetry in the plane of interfaces requires that the two-dimensional (2D) reciprocal-lattice vectors $\mathbf{k}_{\|}$ be conserved, so that equation (2) holds for each separate $\mathbf{k}_{\|}$ channel and all quantities in equation (2) are $\mathbf{k}_{\|}$ resolved. In this case we rewrite it as

$$\begin{aligned}G &= \frac{j}{W} \\ &= \frac{2\pi e^2}{\hbar}\mathrm{Tr}\,[\rho^{\alpha}(\epsilon_{\mathrm{F}},\mathbf{k}_{\|})[\mathbf{t}^{\dagger}]^{\alpha\beta}(\epsilon_{\mathrm{F}},\mathbf{k}_{\|})\rho^{\beta}(\epsilon_{\mathrm{F}},\mathbf{k}_{\|})t^{\beta\alpha}(\epsilon_{\mathrm{F}},\mathbf{k}_{\|})].\end{aligned} \tag{6}$$

To obtain the total conductance it is necessary to sum over $\mathbf{k}_{\|}$ in the 2D Brillouin zone (BZ). In the following discussions the $\mathbf{k}_{\|}$ argument is suppressed and all quantities are $\mathbf{k}_{\|}$ resolved unless otherwise stated. For rough electrode–barrier interfaces or scattering by defects there is no $\mathbf{k}_{\|}$ conservation, and the $\boldsymbol{\rho}$, **V** and **G** matrices in the following equation (8) are separately summed over $\mathbf{k}_{\|}$ before integrating over energy (Caroli *et al.* 1971).

For spin-polarized systems the direction of the conduction electron's spin is conserved as we have not considered any spin-flip scattering processes. Therefore, equation (6) holds for each spin channel, and the JMR ratio is defined as

$$\mathrm{JMR} = \frac{G_{\uparrow\uparrow} + G_{\downarrow\downarrow} - G_{\uparrow\downarrow} - G_{\downarrow\uparrow}}{G_{\uparrow\uparrow} + G_{\downarrow\downarrow}}, \tag{7}$$

where $G_{\sigma,\sigma'}$ is the conductance for one spin channel when the moments of the two electrodes are aligned parallel or antiparallel to one another. In the following discussions spin indices are also suppressed.

An equivalent expression for the conductance is found by inserting equation (4) into equation (2) and we have

$$\mathbf{G} = \frac{4\pi^2 e^2}{h} \mathrm{Tr}\,[\rho^{\alpha} V^{\alpha a} (G^{\dagger})^{ab} V^{b\beta} \rho^{\beta} V^{\beta b} G^{ba} V^{a\alpha}], \tag{8}$$

where now all the quantities in the parentheses are 9×9 matrices with angular momentum indices; the latter arises as follows. To incorporate the results of *ab initio* SKKR calculations into the tight-binding formalism for the conductance, an appropriate discrete basis set $|iL\rangle$ has to be employed; here i denotes the layer index and $L \equiv (lm)$ are angular momentum indices. As we consider s, p and d states we have nine states altogether.

There are two ways of proceeding: either by finding the **t** matrix directly and using equation (2) or by finding the hopping integrals $V^{\alpha a}$ and propagator G^{ab} and using equation (8). As we have the full Green's functions for the entire junction from *ab initio* calculations we obtain the **t** matrix $t^{\beta\alpha}$ from Dyson's equation $\mathbf{G} = \mathbf{g} + \mathbf{gVG} = \mathbf{g} + \mathbf{gtg}$. As there is little to no coupling across the layers α and β, that is the barrier, in the unperturbed (isolated) system the unperturbed propagator $g^{\beta\alpha}$ is zero, and

$$G^{\beta\alpha} = \sum_{\alpha',\beta'} g^{\beta\beta'} t^{\beta'\alpha'} g^{\alpha'\alpha}. \tag{9}$$

As it stands this expression is not easily inverted to find the **t** matrix; however, if we assume that the tight-binding description is a reasonable albeit uncontrolled approximation for $G^{\beta\alpha}$ we find in our calculations that we can use equation (4) to reduce equation (9) to

$$G^{\beta\alpha} = g^{\beta\beta} t^{\beta\alpha} g^{\alpha\alpha}. \tag{10}$$

Now $t^{\beta\alpha}$ can be obtained by inversion:

$$t^{\beta\alpha} = (g^{\beta\beta})^{-1} G^{\beta\alpha} (g^{\alpha\alpha})^{-1}. \tag{11}$$

By placing this into equation (2), we obtain the following expression for the tunnelling conductance:

$$\mathbf{G} = \frac{4\pi^2 e^2}{h} \mathrm{Tr}\,[\rho^{\alpha} (g^{\dagger\alpha\alpha})^{-1} (G^{\dagger})^{\alpha\beta} (g^{\dagger\beta\beta})^{-1} \times \rho^{\beta} (g^{\beta\beta})^{-1} G^{\beta\alpha} (g^{\alpha\alpha})^{-1}]. \tag{12}$$

The hopping integrals do not appear here, because all the coupling and barrier information is contained in $G^{\beta\alpha}$. The other method of evaluating the conductance via equation (8) is discussed in detail in appendix A. Equation (12) is more amenable to numerical calculations as long as one can calculate $G^{\beta\alpha}$ directly because the reduced numerical matrix manipulations (as opposed to the other approach) means higher accuracy. In concluding this discussion of equation (6), we point out that, when it is applied to calculating the conductance of a barrier one does take into account in $t^{\beta\alpha}$ how it couples to the states in the electrodes. In this manner, as well as through ρ^{α} and ρ^{β}, the influence of spin polarization in the electrodes enters the conductance of an otherwise spin-unpolarized barrier.

§ 3. Defining the Green's functions

The SKKR method generates the Green's function in continuous space as follows:

$$G(\mathbf{r},\mathbf{r}',\epsilon)=\sum_{LL'}[Z_l^i(\epsilon,r_i)\,Y_{lm}^*(\hat{\mathbf{r}}_i)\tau_{LL'}^{ij}(\epsilon)Z_{l'}^j(\epsilon,r_j')\,Y_{l'm'}(\hat{\mathbf{r}}_j')$$
$$-\delta^{ij}\delta_{LL'}Z_l^i(\epsilon,r_<)\,Y_{lm}(\hat{\mathbf{r}}_<)J_l^j(\epsilon,r_>)\,Y_{lm}^*(\hat{\mathbf{r}}_>)]$$

where $\mathbf{r}$ is located in atomic cell i, $\mathbf{r}'$ is located in atomic cell j; $\mathbf{r}=\mathbf{R}_i+\mathbf{r}_i$, $\mathbf{r}'=\mathbf{R}_j+\mathbf{r}_j'$, and $\mathbf{R}_i$ and $\mathbf{R}_j$ are Bravais lattice vectors; $r_>$ ($r_<$) refers to the larger (smaller) of r_i and r_j'; $J_l^i(\epsilon,r)$ is an irregular solution to the Kohn–Sham equation.

To incorporate these continuous real-space Green's functions into the conductance formula which was derived in a tight binding description, we need to find an appropriate layer-dependent basis set. Because conductance is a trace over all possible indices, in principle it should not depend on which base one chooses to express the Green's functions, as long as it is orthonormal, complete and relatively localized; however, in reality, different choices of basis set lead to slightly different results, because only the nearest neighbours are included in our calculations, albeit in a principal layer description. The basis that we find most natural and convenient to use is the normalized muffin-tin part of the scattering solutions from the Korringu–Kohn–Rostoker calculation, which is the regular solution to the Schrödinger equation within an atomic cell i of radius R_s in the atomic sphere approximation (ASA) sense (Weinberger 1990) and zero outside:

$$\langle\mathbf{r}|iL\rangle=\phi_l^i(r)\,Y_{lm}(\hat{\mathbf{r}})=CZ_l^i(r)\,Y_{lm}(\hat{\mathbf{r}})\Theta(R_s-r),\tag{13}$$

which is defined within atomic cell i. Here C is a normalization constant for each cell; in terms of this basis set, for $i\neq j$ we have

$$\begin{aligned}G_{LL'}^{ij}&=\langle iL|\mathbf{G}|jL'\rangle\\&=\int_{\Omega_i}\mathrm{d}\mathbf{r}\int_{\Omega_j}\mathrm{d}\mathbf{r}'\,\langle iL|\mathbf{r}\rangle\mathbf{G}(\mathbf{r},\mathbf{r}')\langle\mathbf{r}'|jL'\rangle\\&=\int_{\Omega_i}\mathrm{d}\mathbf{r}\int_{\Omega_j}\mathrm{d}\mathbf{r}'\,\phi_l^{i*}(r)\,Y_{lm}^*(\hat{r})\phi_{l'}^j(r')\,Y_{l'm'}(\hat{r}')\\&\quad\times\sum_{QQ'}Z_q^i(r)\,Y_{qm_q}(\hat{r})\tau_{QQ'}^{ij}Z_{q'}^j(r')\,Y_{q'm_q'}^*(\hat{r}')\\&=\int_{\Omega_i}\phi_l^{i*}(r)Z_l^i(r)r^2\,\mathrm{d}r\,\tau_{lm,l'm'}^{ij}\\&\quad\times\int_{\Omega_j}Z_{l'}^j(r')\phi_{l'}^j(r')r'^2\,\mathrm{d}r'\end{aligned}$$

while, for $i=j$, there is a second term

$$-\int_{\Omega_i}\phi_l^{i*}(r)Z_l^i(r)r^2\,\mathrm{d}r\int_{\Omega_i}J_l^j(r')\phi_l^j(r')r'^2\,\mathrm{d}r'$$
$$\times\delta^{ij}\delta_{LL'}\Theta(r'-r)+(Z\longleftrightarrow J).\tag{14}$$

Here τ^{ij} is the so-called scattering path operator, and $J_l^j(r)$ is the irregular solution to the Schrödinger equation in atomic cell j. Clearly $\operatorname{Im}G_{LL}^{ii}=\operatorname{Im}[\int_{\Omega_i}G_{LL}(\mathbf{r},\mathbf{r})\,\mathrm{d}\mathbf{r}]$.

From a SKKR calculation we only find the Green's functions for the entire coupled junction; to obtain the isolated electrode Green's functions $g^{\alpha\alpha}$ and $g^{\beta\beta}$ as well as coupling matrices (hopping integrals) required in the conductance calcula-

tion, we can make use of Dyson's equation applied to sites across an interface under the assumption of nearest-neighbour (within a principal layer description) hopping:

$$\begin{aligned} G^{\alpha\alpha} &= g^{\alpha\alpha} + g^{\alpha\alpha} V^{\alpha a} G^{a\alpha}, \\ G^{aa} &= g^{aa} + g^{aa} V^{a\alpha} G^{\alpha a}, \\ G^{\alpha a} &= g^{\alpha\alpha} V^{\alpha a} G^{aa}, \\ G^{a\alpha} &= g^{aa} V^{a\alpha} G^{\alpha\alpha}. \end{aligned} \tag{15}$$

These equations can be solved to find the **g** and **V** components as follows:

$$\begin{aligned} g^{\alpha\alpha} &= G^{\alpha\alpha} - G^{\alpha a} (G^{aa})^{-1} G^{a\alpha}, \\ V^{\alpha a} &= [g^{\alpha\alpha}]^{-1} G^{\alpha a} [G^{aa}]^{-1}, \\ g^{aa} &= G^{aa} - G^{a\alpha} [G^{\alpha\alpha}]^{-1} G^{\alpha a}, \\ V^{a\alpha} &= [g^{aa}]^{-1} G^{a\alpha} [G^{\alpha\alpha}]^{-1}. \end{aligned} \tag{16}$$

We reiterate that, in all the discussions above, we have assumed that only the nearest-neighbour coupling is included across the interfaces, that is the tight-binding description; in principle the whole formalism is also valid if more distant neighbours are also included. This is accomplished by using principal layers with the desired number of atomic layers in each principal layer (Mathon 1997, Mathon and Umerski 2001). As interactions with more distant neighbours are included, the calculations become increasingly cumbersome; therefore we have limited our consideration to interactions only between nearest-neighbour principal layers.

§ 4. Calculations and results

Calculations were made for bcc Fe(100)/vacuum/Fe(100), for fcc Co(100)/vacuum/Co(100) and fcc Ni(100)/vacuum/Ni(100) tunnel junctions. The band structures were obtained from spin-polarized scalar-relativistic SKKR calculations, and the ASA is used. The lattice parameters for Fe, Co and Ni are 5.27, 6.55 and 6.56 au respectively, and the screening potential is set to 2 Ry inside each atomic cell. While three atomic layers are included in each principal layer in the screened configuration, in conductance calculations only two atomic layers are included in a principal layer when coupling to the second-nearest neighbour is considered. The Gunnarsson–Lundqvist (1976) exchange–correlation potential is used, and energy integration is performed by means of Gaussian quadrature with 16 points on a semicircle in the upper half of the complex energy plane. For self-consistent calculations of the bulk metal, the free metal surface and the metal/vacuum/metal interface potentials, 45 $\mathbf{k}_\parallel$ points are used in the irreducible wedge of the first 2D BZ, which enables the Fermi level to be converged up to 10^{-7} Ry. For more details on this method, see Szunyogh *et al*. (1994).

In calculating the Green's functions and conductances, 90 000, 40 000 and 57 600 $\mathbf{k}_\parallel$ points in the whole 2D BZ are used for the minority-spin channel, respectively for the majority-spin channel and for the antiparallel alignment of the moments of the electrodes. A larger number of points were used for the minority channel calculation because the **k**-space distribution of the Green's functions and hence of the integrand in equation (6) is much more sharply peaked for this channel than for the other cases. Convergence is tested by comparing these results with the results using 115 600 $\mathbf{k}_\parallel$ points; we found that differences for each channel were well within 1%. One should use the smallest possible value for the imaginary part of the complex energy,

δ; however, if it is too small, both the number of iterations required to make the structure constants converge and the number of $\mathbf{k}_{\|}$ points required to make physical quantities converge are too large for us to perform. In our calculation a value of 5×10^{-4} Ry is used. This may not be small enough for all the conductance calculations; however, when we compare our results for bulk metal as discussed below with those found by using $\delta = 10^{-3}$ Ry the conductance is essentially unchanged. For tunnelling conductance an increase of about 10% with the smaller δ is observed for the minority-spin channel, while increases for the majority-spin and antiparallel conductances are much smaller. These differences diminish for thicker barriers, so that JMR values obtained here should be regarded as lower limits of the JMR for each barrier thickness considered. In all the conductance calculations, couplings up to second nearest neighbours across the interfaces are included.

4.1. *Bulk metal ballistic conductance*

To test our methods for defining the Green's functions and deriving the isolated electrode Green's functions and hopping integrals that enter the conductance formula as shown in §§ 2 and 3, we calculated the ballistic conductance of bulk Co for energies around the Fermi level. To implement the Caroli *et al.* formalism we made an artificial cut through the bulk metal and derived $\mathbf{g}$ and $\mathbf{V}$ across this cut by using equations (16); then equation (6) is used to calculate the conductance. The results are shown in figure 1 (*d*), together with the variation with energy of the spin-polarized DOSs for bulk Co, the free surface layer of Co and the isolated surface layer of Co electrode. Again by an *isolated surface* we mean one terminated so that there is no electron transfer from the surface (Pollmann and Pantelides 1978); this can also be achieved for example by setting the hopping integrals across the interface to zero. For a free surface, electrons escape from the metallic electrode into the vacuum; in figure 2 we compare the three types of $\mathbf{k}_{\|}$ resolved DOS at the Fermi level. The values for the conductance agree reasonably well with the Co conductance calculation by Mathon *et al.* (1997) in the whole energy range we have investigated; for example, with two atomic layers in each principal layer, their conductance values for the majority and minority at the Fermi level are around 0.7 and 1.9 compared with our values of 0.71 and 1.97 in units of e^2/h.

We also calculated the ballistic conductances for bulk Ni and bcc Fe at the Fermi level; numerical results are shown in table 1, together with the DOS at the Fermi level for the bulk metal, a free surface layer, an isolated surface layer of the electrode and the first vacuum layer. In figure 3 we compare the three types of $\mathbf{k}_{\|}$-resolved DOS at the Fermi level for Fe. The corresponding plots for Ni are similar to those for Co; so we shall not repeat them here. The DOS for the isolated electrode layers resembles the free surface DOS much more than the bulk DOS. This is to be expected, since the surface of an isolated electrode is just a special way of terminating or defining a surface. This point is especially apparent for Fe, where a reversal is obtained in the spin polarization for the d-electron DOS at the Fermi level for both free and isolated surfaces compared with the bulk value. As shown in these plots, the majority channel DOS is smooth and the minority channel DOS is extremely spiky for Co for all three kinds of layer, while for Fe this difference is less distinctive; for example, the majority DOS is more spiky than the minority DOS for the bulk in contrast with the situation in the two kinds of surface layer. For Fe, the isolated surface DOS is less (negatively) polarized than that of the free surface, while for Co and Ni they are more polarized than those of the free surfaces.

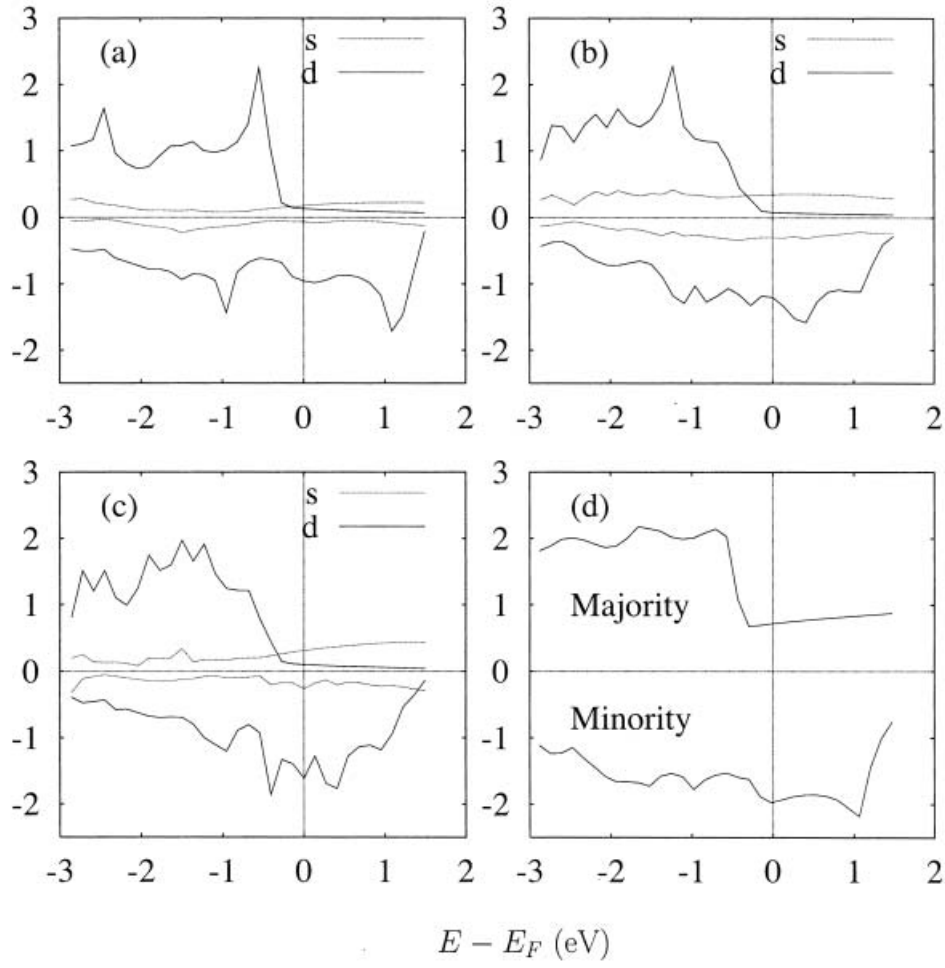

Figure 1. (*a*) Bulk Co DOS, (*b*) free surface Co layer DOS, (*c*) isolated electrode surface Co layer DOS and (*d*) ballistic conductance of bulk Co around the Fermi level. The units for the DOSs are states $\text{atom}^{-1}\,\text{eV}^{-1}$ and the units for conductance are e^2/h. The DOS plots for the s electrons are enlarged 15 times so that one can see them on the same plot as the DOS plots for the d electrons.

We have not been able to achieve convergence for the bulk conductance with respect to the number of nearest neighbours included in all our calculations. In calculations where we included third-nearest neighbours, the bulk conductances in each spin channel increased by about 20% for Co and Ni, while for Fe it remained essentially unchanged. These changes can be understood by assuming that the coupling across the artificial cut in the metal goes beyond nearest neighbours. For Fe, because of the reversal of the polarization of DOS in the surface layer, the inclusion of more layers tends to reduce the influence of this reversal and hence to stabilize the

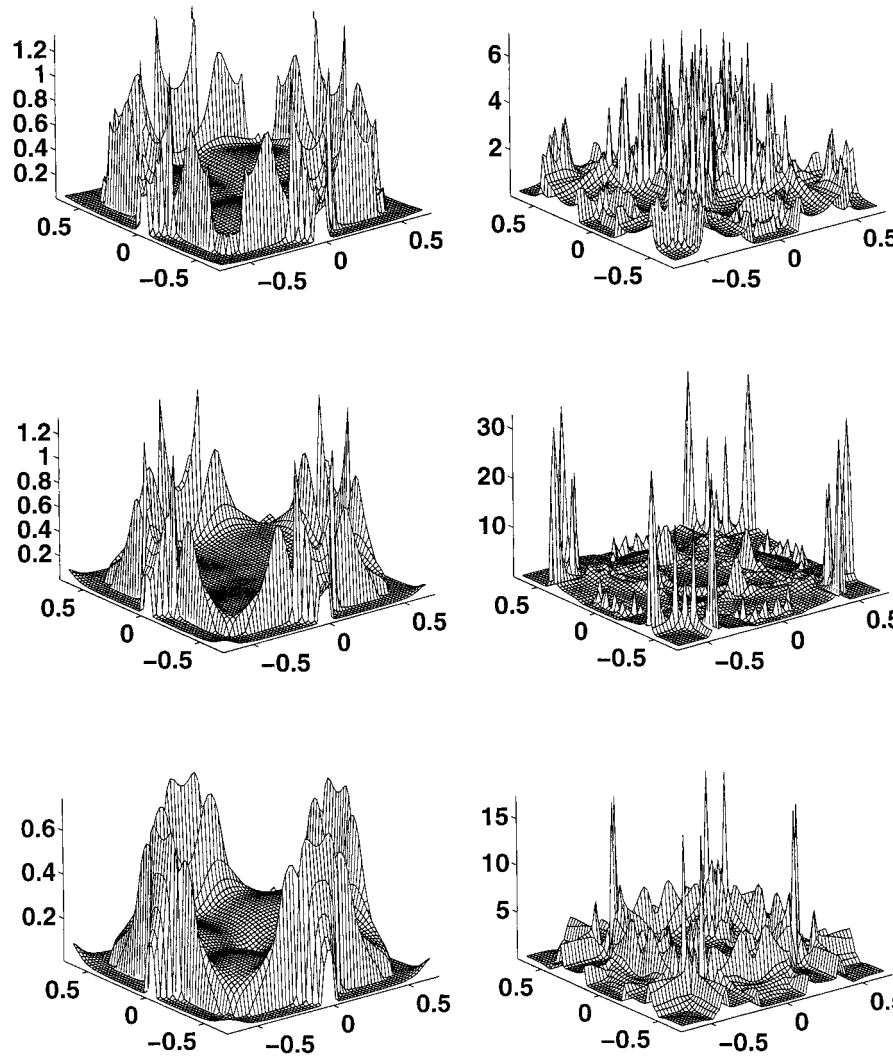

Figure 2. $\mathbf{k}_{\|}$-resolved (partial) DOSs in units of states atom^{-1} eV^{-1} of fcc Co(100) plotted in the first 2D BZ. The left-hand column is for the majority-spin channel and the right-hand column is for the minority-spin channel. From top to bottom, the DOSs for a bulk Co layer, a free surface Co layer and the isolated electrode surface Co layer are shown. Colour contour plots of these figures can be viewed at http://physics.nyu.edu/~pl2/.

results while, for Co and Ni, there are no radical differences between surface and inner layers; thus including more inner layers will only increase the conductance values, especially for the parallel configuration. Nevertheless, the inclusion of second nearest neighbours should give a reasonable approximation, especially for tunnelling across a finite barrier where the coupling between the electrodes and the barrier is even shorter ranged.

Parenthetically, by using the Caroli *et al.* formalism to calculate the conductance of a metallic structure we encounter difficulties arising from current driven charge

Table 1. Spin-polarized DOSs at the Fermi level for a bulk layer, a free surface layer, an isolated surface layer and the first vacuum layer in Fe, Co and Ni tunnel junctions, and spin-polarized conductances of *bulk* Fe, Co and Ni metals. An upward-pointing arrow denotes the majority channel, and a downward-pointing arrow the minority channel.

	ρ^{bulk} (states atom^{-1} Ry^{-1})	ρ^{surface} (states atom^{-1} Ry^{-1})	$\rho^{\text{electrode}}$ (states atom^{-1} Ry^{-1})	ρ^{vacuum} (states atom^{-1} Ry^{-1})	G^{bulk} (units of e^2/h)
Fe↑	10.23	3.94	7.95	0.56	2.06
Fe↓	3.27	19.61	16.55	1.79	1.16
Co↑	2.42	1.83	1.83	0.38	0.71
Co↓	13.42	17.75	22.86	1.04	1.97
Ni↑	2.47	4.22	1.92	0.34	0.74
Ni↓	20.59	22.34	18.57	0.60	2.13

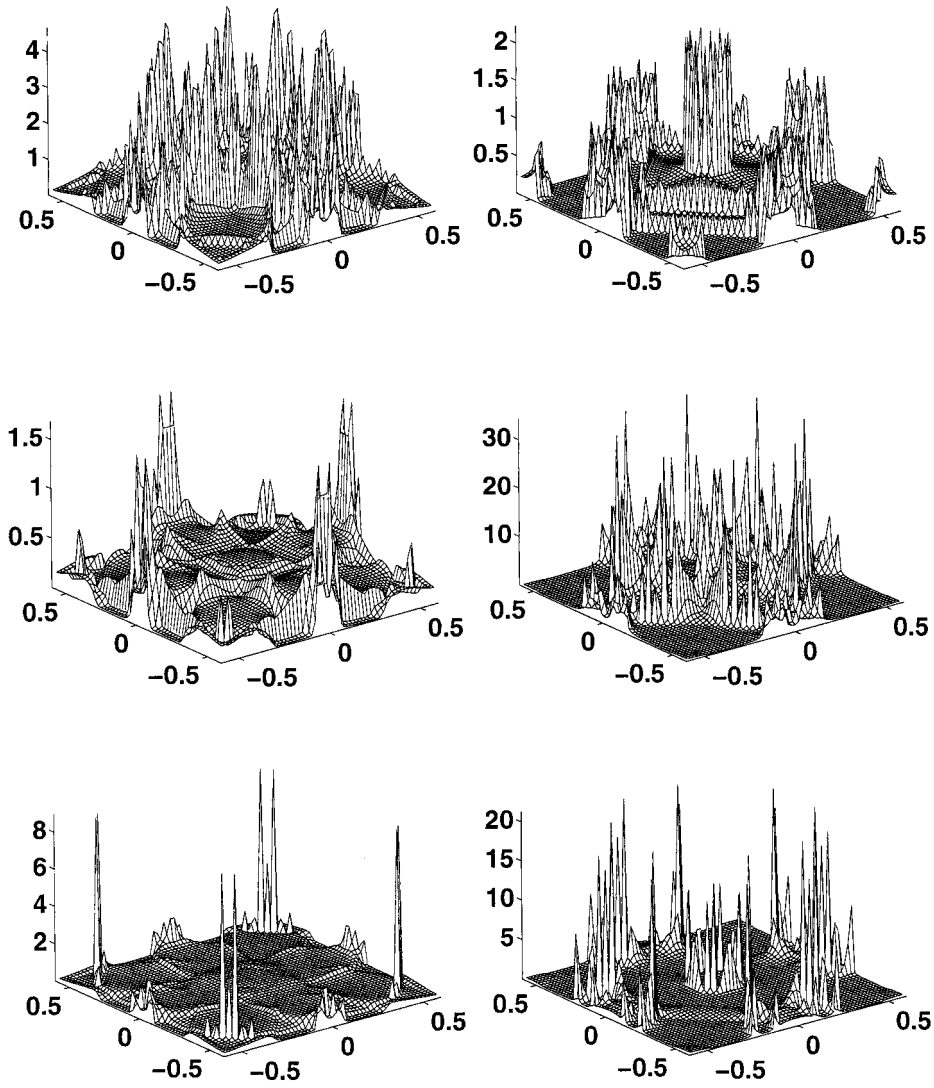

Figure 3. $\mathbf{k}_{\|}$-resolved (partial) DOSs in units of states atom^{-1} eV^{-1} of bcc Fe(100) plotted in the first 2D BZ. The left-hand column is for the majority-spin channel and the right-hand column is for the minority-spin channel. From top to bottom, the DOSs for a bulk Fe layer, a free surface Fe layer and the isolated electrode surface Fe layer are shown. Colour contour plots of these figures can be viewed at http://physics.nyu.edu/~pl2/.

and spin accumulation that are not present in tunnelling junctions (for example Weinberger *et al.* (2001)). Therefore it is not useful to draw too many conclusions about the applicability of our formalism for calculating the conductance of tunnel junctions from these tests on bulk metals.

4.2. *Density of states*

To make our analysis of the JMR calculation results in the next section clearer, we first discuss our results on the spin-polarized DOS of the Fe(6)–vacuum(6) and

Co(6)–vacuum(6) interfaces for two layers on either side of the interface, which have been decomposed into angular momentum components: s, p and d. While this decomposition is reasonable for the metal layers, it is less so for the vacuum layers as there is no positive charge at the centre of the cells to attract the electrons; therefore for the vacuum layers we only show the total DOS. We do not show the DOS of the Ni(6)–vacuum(6) interface because it has a similar structure to that of Co. We have calculated the DOS for free surfaces of Fe, Co and Ni in the highly symmetric (100), (110) and (111) crystallographic directions.

In figure 4 the DOSs around the Fermi level in the metal layers and vacuum (empty cell) layers near the bcc Fe free metal surface in these three directions are plotted. For convenience of visualization, for the metal layers only the s and d partial DOSs are plotted while, for the vacuum layers, only the total DOSs are plotted for the reasons mentioned above. For metal layers, the d DOS is much larger than the s DOS while, in the vacuum layers, although not shown, the difference is very small and usually the s DOS dominates. In the inner metal layers, that is bulk, of Fe both s and d DOSs are positively polarized (and of course, for bulk metal layers, there should be no directional dependence of DOS); as we approach the surface, a directional dependence shows up as one would expect from the fact that different surface directions have different 2D lattice structures and therefore different electron distributions and different work functions.

In the (100) direction for Fe, the s DOS is positively polarized in all metal layers because of the strong s–d mixing, and the Fermi level is inside both majority and minority d bands. The d-band DOS, while positively polarized in the bulk of Fe, is negatively polarized in the surface layer. In the vacuum layers, because of the influence of the surface metal layer, that is leakage of electrons from the surface of the metal into the vacuum, the DOS at the Fermi level is negatively polarized for both s and d bands and therefore also for the total. The peaks in the DOS, although small, are particular to the (100) and (111) surfaces of bcc Fe metal and have been used to explain some anomalous STM experiment results (Krans and van Rutenbeek 2002). The sign of the polarization does change when one places a layer of O on top of the Fe surface (Nguyen-Manh *et al*. 1998, Tsymbal *et al*. 2000).

The (111) direction shows a similar DOS and polarization profile as the (100) direction, while the (110) direction shows a somewhat different profile from these two directions in that in the surface metal layers, both s and d DOSs are essentially unpolarized, and the charge transfer to the vacuum is much smaller than in the other two directions. These differences can be understood by noting the varying interlayer distances. For Fe, the cubic lattice constant is 5.27 au; the layer-to-layer distance in the (111) directions is 1.52 au (2D hexagonal lattice), in the (100) direction it is 2.64 au (square lattice) and in the (110) direction it is 3.73 au (centred rectangular lattice). So we see that a (111) surface has the smallest distance between layers in the growth direction, and therefore more overlap between primitive cell atomic wavefunctions in this direction; hence more electrons are transferred to the vacuum layers. A (110) surface has just the opposite behaviour. The consequences of the differences in surface lattice structure lies in every aspect of the charge and magnetic moment distribution. For instance, the work functions also show clearly the differences: for a (110) surface, it is 0.40 Ry, for a (100) surface, it is 0.37 Ry while, for a (111) surface, it is only 0.32 Ry.

In figure 5 we show the same plots for fcc Co surfaces in the three directions. Here the directional dependence in the metal layers is not significant and from bulk

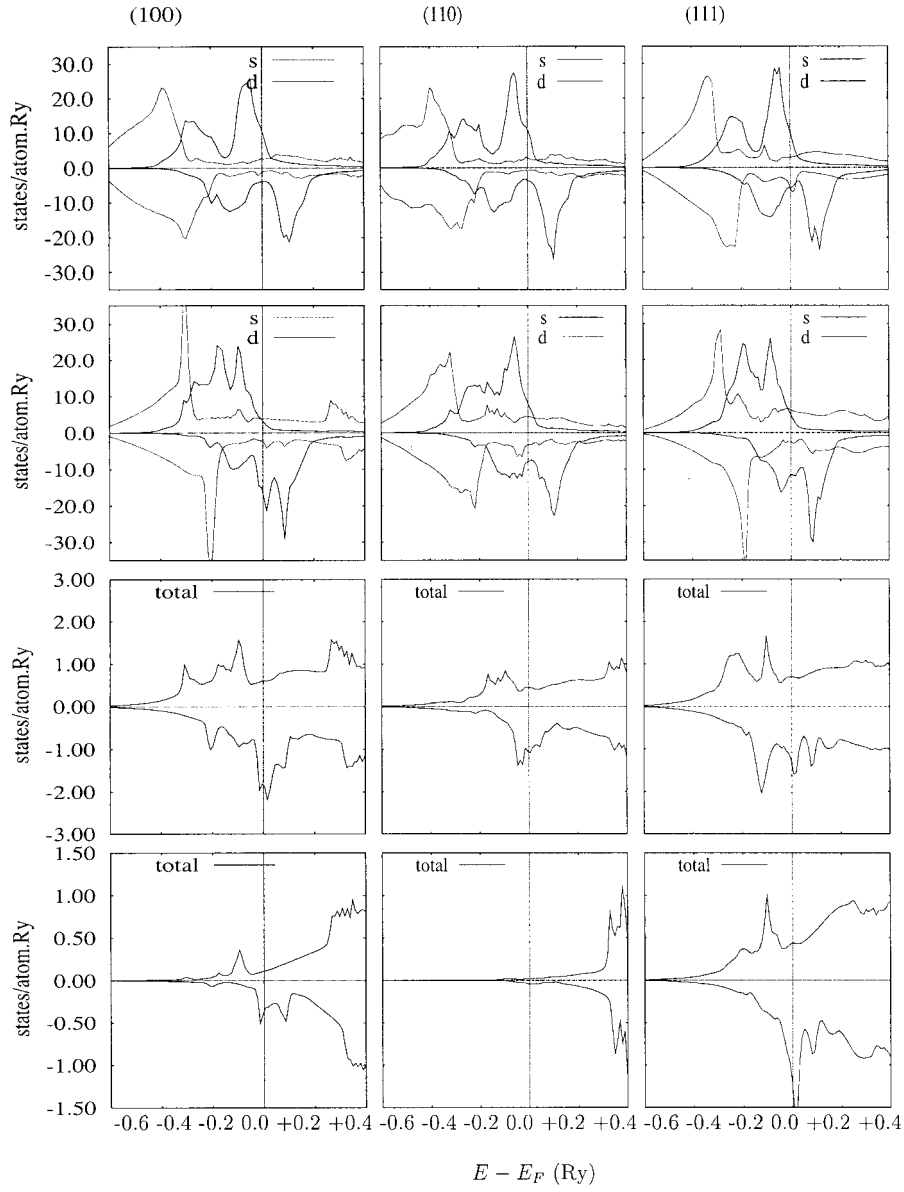

Figure 4. Angular-momentum-resolved DOSs around the Fermi level of a bcc Fe surface in the (100), (110) and (111) directions. From top to bottom the DOSs are shown for the next-to-surface Fe layer, the surface Fe layer, the first vacuum layer and the second vacuum layer. In the Fe layers the s component is enlarged 15 times.

layers to surface layers the change in DOS and polarization is very small, mainly because the Fermi level always lies above the majority d bands but within the minority d channel. The s-band DOS is always positively polarized while the *d*-band DOS is always negatively polarized in the metal layers. Again, in the vacuum layers, because of the negative spin polarization in the metal layers, polarization is negative, and the strong directional dependence can be explained by the large differ-

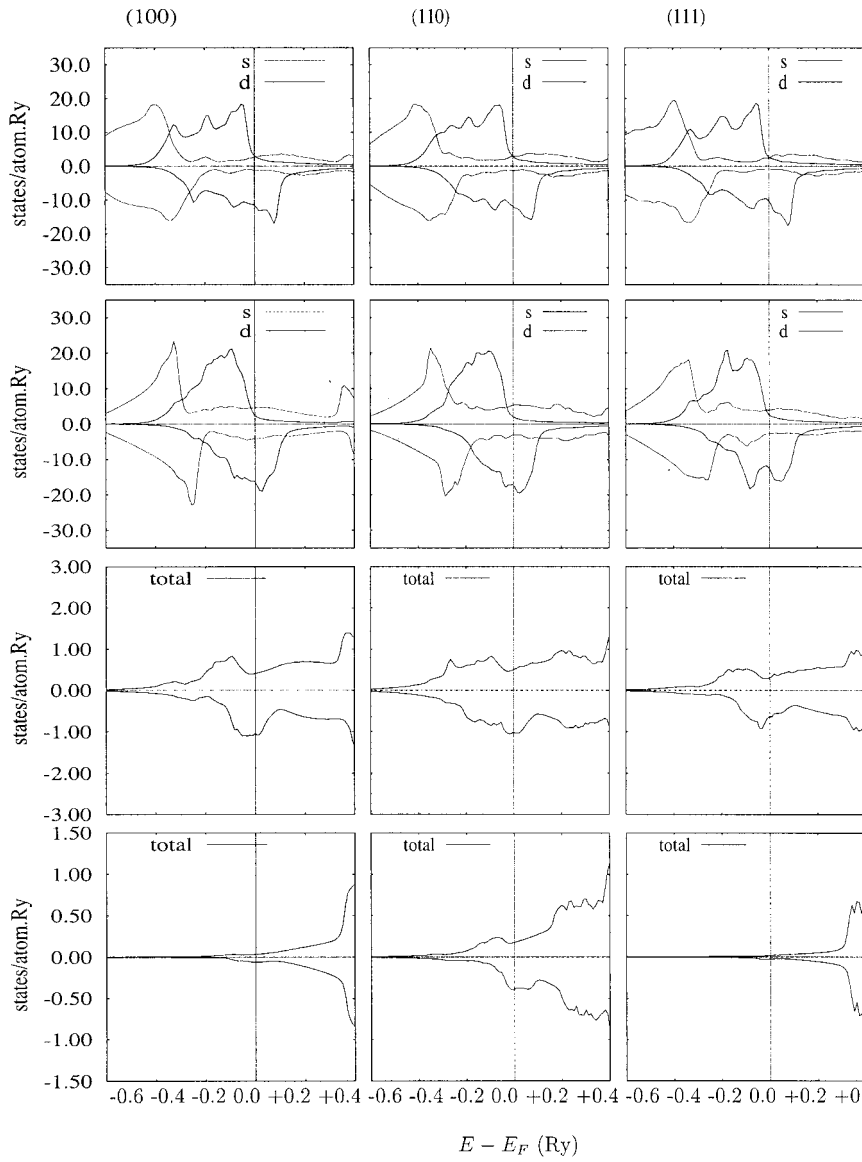

Figure 5. Angular-momentum-resolved DOS around the Fermi level of a bcc Co surface in the (100), (110) and (111) directions. From top to bottom the DOSs are shown for the next-to-surface Co layer, the surface Co layer, the first vacuum layer and the second vacuum layer. In the Co layers the s component is enlarged 15 times.

ences in the surface (2D) lattice structures and the different interlayer distances. Here the (110) direction has the shortest interlayer distance (2.31 au) and hence the largest transfer of electrons. The (111) direction has the largest interlayer distance (3.27 au, close to the one for the (100) direction) and hence the smallest transfer.

As we discuss below, the conductance values for thick barriers, although not directly proportional to the product of the surface DOS of the two electrodes, do seem to be positively correlated to them. For thinner barriers, the situation is more

complicated and such a conclusion cannot be drawn; because of the strong direct coupling between the two electrodes (wavefunction overlap), the barrier is significantly modified.

4.3. *Tunnelling conductance and magnetoresistance*

Calculations of tunnelling conductance *for the barrier region alone* were made for bcc Fe(100)/vacuum/Fe(100) for fcc Co(100)/vacuum/Co(100) and fcc Ni(100)/vacuum/Ni(100) tunnel junctions. Convergence tests with the number of nearest neighbours show that, in the tunnelling calculations, inclusion of the second-nearest neighbour suffices; this indicates that hopping across the metal–vacuum interface indeed *is* quite short ranged.

In figure 6(*a*), (*b*) and (*c*), we show the distribution of tunnelling conductance in the first 2D BZ for majority-spin, minority-spin and antiparallel configurations respectively in a Co junction when the thickness of the vacuum is six atomic layers. Although in conductance calculations we used an energy imaginary part of $\delta = 0.5\,\mathrm{mRy}$, an imaginary part of 5 mRy for the energy is used in these plots so that they will not appear too spiky, particularly in the minority channel. The distribution for majority spin conductance resembles that of free electron tunnelling across a constant potential barrier (Butler *et al.* 1997, 2001, MacLaren *et al.* 1997, 1999) and is dominated by tunnelling states in the centre of the 2D BZ. The minority-spin channel conductance has a more complex structure; it is dominated by only a few $\mathbf{k}_{\|}$ states. These same features also appear in tunnelling across insulators (for example Butler *et al.* (1997, 2001) and MacLaren *et al.* (1997, 1999)); only here the minority-spin channel for our vacuum barrier has a much higher conductance whereas one finds that for junctions with Al_2O_3 the majority channel has higher conductance. From table 1 we see that, in the vacuum layer adjacent to the metal surface, the total DOS for minority electrons is about three times that for majority electrons. This is in sharp contrast with DOS results for alumina barriers in contact with ferromagnetic metals (Nguyen-Manh *et al.* 1998, Tsymbal *et al.* 2000), where majority electrons have a larger DOS around the Fermi level than minority electrons in the barrier layers near the metal surface. Also more recent studies by Oleinik *et al.* (2000) have found that the DOS at the Fermi level inside an alumina barrier for $Co/Al_2O_3/Co$ junctions gradually change sign as one goes to the central layer; they thereby infer that the tunnelling current will have majority-spin polarization for alumina barriers thicker than 10–12 monolayers (ML).

Plots of the changes in the JMR ratio with the number of vacuum layers are shown in figure 7 for the three tunnel junctions. Changes in JMR with the barrier thickness are the result of the combined effect of the barrier band structure and the coupling of the various bands of the metal into the vacuum barrier (which owing to charge transfer also leads to the vacuum barrier electronic structure). For vacuum barriers with only a few layers, the JMR is strongly influenced by the spill-over of charge from the metal; as a result for Co there is a dip around two atomic layers. For thicker barriers, as we mentioned, the vacuum barrier is for the most part a potential plateau and the changes in JMR with the vacuum thickness is mainly the result of the different couplings of the metal s, p and d bands, that is the states at the electrode–barrier interface, into the barrier bands. Whether the JMR increases or decreases with the vacuum barrier thickness depends on the multiband structures of the barrier. For Co/vacuum/Co junctions it is a decreasing function of barrier thickness. At 12 atomic layers, the JMR is about 18%. Recent studies by Butler *et al.* (2001)

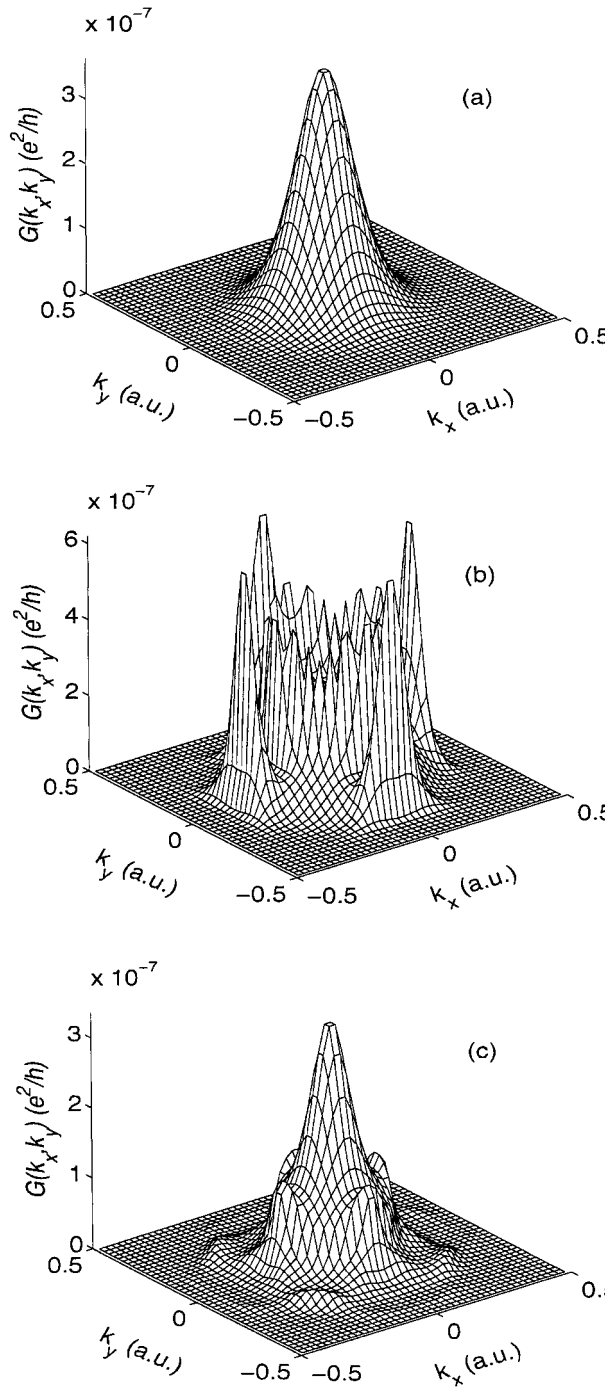

Figure 6. $\mathbf{k}_{\|}$-resolved (partial) tunnelling conductance of the barrier region of a Co junction in the first 2D BZ when the magnetizations of the two electrodes are aligned (*a*) in parallel for the majority-spin channel, (*b*) in parallel for the minority-spin channel and (*c*) antiparallel. The vacuum barrier is six atomic layers thick. Colour contour plots of these figures can be view at http://physics.nyu.edu/~pl2/.

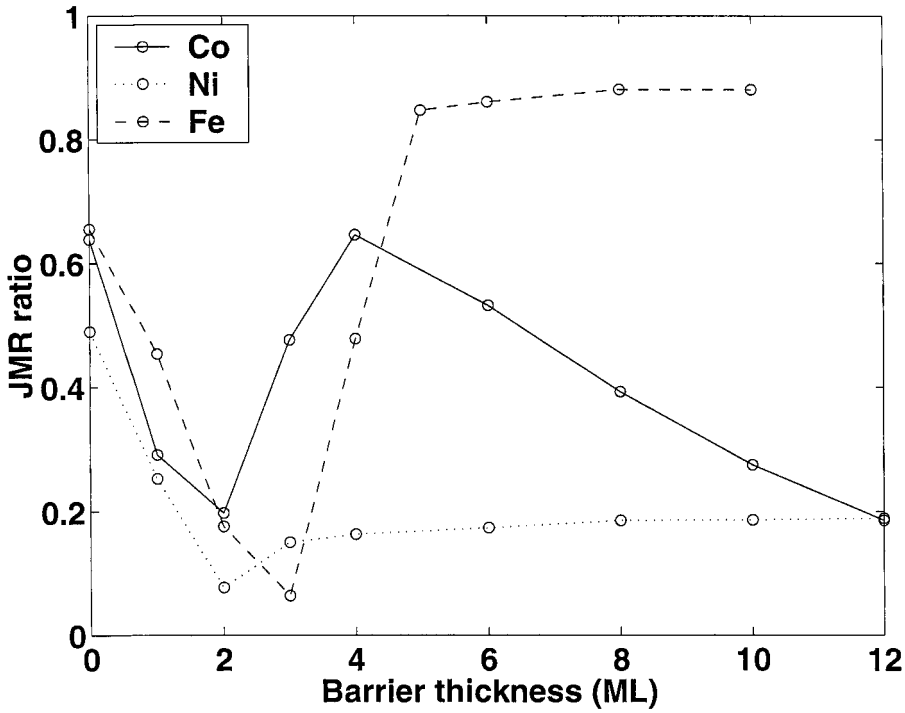

Figure 7. JMR ratio change with the barrier (vacuum) thickness in fcc Co(100), fcc Ni(100) and bcc Fe(100) tunnel junctions when calculating the conductances only for the barrier regions.

indicated that, by using the ASA for the vacuum layers, one does not obtain a realistic assessment of the decay of states with different orbital character in the barrier. For this reason some of the details of the above results may be artefacts of our having used the ASA for the vacuum.

Changes in JMR with the vacuum barrier thickness for the Ni junction are very similar to those for the Co junction because fcc Ni and Co have very similar band structures. The work function of Ni is 5.8 eV, very close to that of Co, and the conductances also decay at a rate similar to that of Co junction. The dip structure in the JMR versus thickness relation is also similar to that of Co junction but, after the dip, the JMR slowly increases instead of decreasing with barrier thickness. At 12 atomic layers the JMR approaches 19%.

The same calculation for the bcc Fe junction shows some different results as would be expected from the DOS results. For small barrier thicknesses the direct overlap of the wavefunctions has the conductance for the majority-spin channel about twice that in the minority-spin channel (see table 1). At about two atomic layers there is a crossover in the conductance, which leads to a dip in the JMR curve at around three atomic layers, after which the minority channel dominates and, at barrier thicknesses larger than six atomic layers, the JMR essentially approaches a saturated value around 80%; this is much higher than corresponding results for Co and Ni junctions. As we mentioned above, some of these features may be artefacts of the ASA that we used for the vacuum. Recent studies by Nguyen-Manh *et al.* (1998) and Tsymbal *et al.* (2000) of the DOS for 1 ML of O on the (100) surface of Fe show

that it is majority spin polarized even though the spin polarization of the Fe (100) is minority dominated; they concluded that the bonding (hopping integrals) at these interfaces is such as to always produce a majority-dominated tunnelling current.

As we have used vacuum as the barrier, our calculations are closely related to STM and field emission (FE) experiments. In STM, experiments on spin-polarized tunnelling involving ferromagnetic metals have been carried out by Alvarado and Renaud (1992), Alvarado (1994, 1995) and Bode *et al*. (1998, 1999) who found that the spin polarizations of tunnelling current from Ni tips into a non-magnetic material are negative in some lattice directions. In FE studies, mixed results were observed, often with strong directional dependences. Although it is hard to link a FE experiment, which involves much higher fields and final states that are quite different from those for tunnelling across vacuum barriers, to our present calculations, the very fact that FE measurements did not yield the almost ubiquitous positive current polarization observed in tunnelling across alumina indicates that the barrier and the coupling are very important factors in tunnelling.

§ 5. Paths of conduction across a junction

The results for the conductance that we have presented were calculated for the barrier region alone. As this is physically a different system from coherent transport across an entire junction as seen in a ballistic calculation, we can anticipate that the results are quite different (Levy *et al*. 2002). Specifically one has, in addition to the considerations above, the problem of matching the states at the electrode–barrier interface to those in the bulk of the electrodes (Butler *et al*. 2001). Therefore we have repeated our above calculations for a bcc Fe(100)/vacuum(10)/Fe(100) tunnel junction with the electrodes at an energy of 0.05 eV below the Fermi energy; we have states localized at the Fe(100)–vacuum interface which form an independent conduction path at this energy (Levy *et al*. 2002), while far away from the barrier the electronic structure reverts to the bulk (frozen, not self-consistently determined) metal potentials. In figures 8 (*a*) and (*b*) we show the $\mathbf{k}_{\|}$-resolved conductance found in this manner plotted across the 2D BZ for the barrier region alone and for the entire junction respectively. Noteworthy differences between the two approaches are as follows.

(i) The symmetry of the $\mathbf{k}_{\|}$ resolved conductance plots are quite different. While the calculation for the barrier alone picks up states localized at the interface along the Γ–X direction, the entire junction ballistic calculation picks up only the resonant states along Γ–M (Butler *et al*. 1997, 2001, MacLaren *et al*. 1997, 1999). In coherent transport across the entire junction the JMR is controlled by these resonances, whereas in our calculations we include the conduction through states localized at the electrode–barrier interfaces.

(ii) The average of the conductance over the 2D BZ is much lower when we assume coherent transport across the entire structure than that for the barrier region alone, for example 0.16×10^{-7} for the former and 0.43×10^{-7} for the latter in units of e^2/h. Our calculations are not conclusive on this difference in magnitudes because the imaginary part of the energy that we use in our propagators acts differently on the itinerant states in the bulk of the electrodes from the localized states at the electrode–barrier interface; also one cannot be sure of the convergence for the number of $\mathbf{k}$ points that we have taken. None the less, this difference is reasonable as one

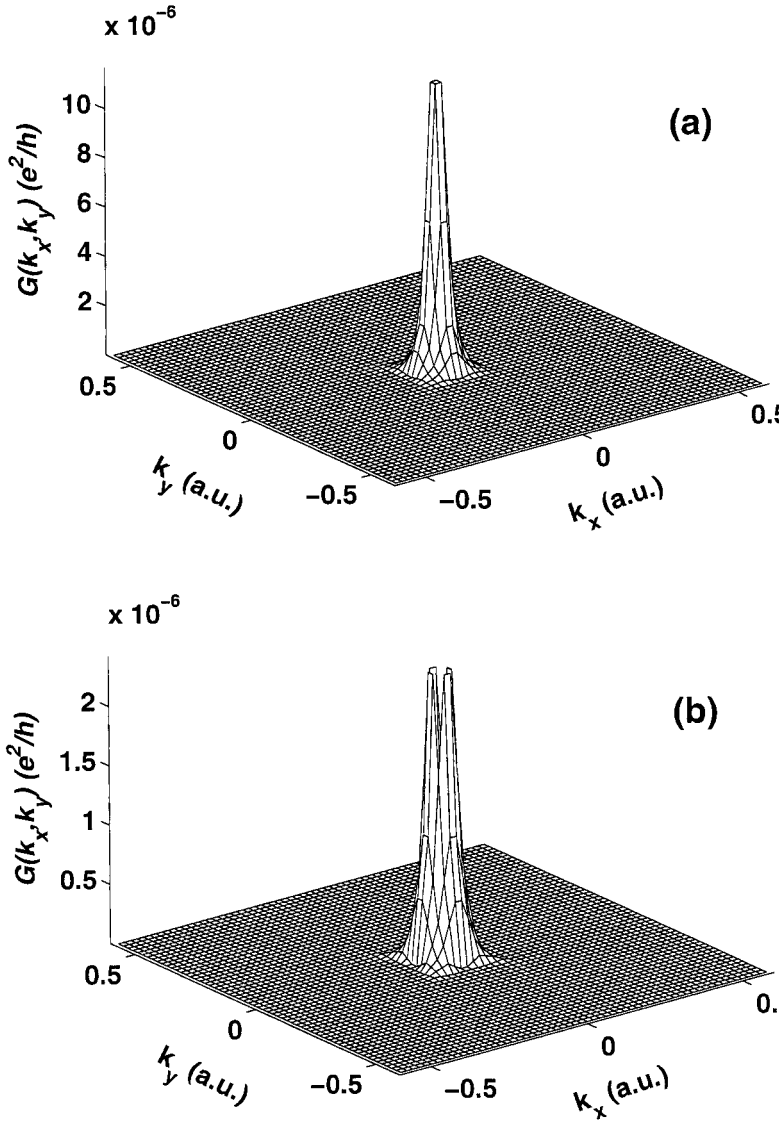

Figure 8. $\mathbf{k}_{\|}$-resolved (partial) tunnelling conductance of bcc Fe(100) vacuum(10)/Fe(100) tunnel junction at an energy 0.05 eV below the Fermi level (*a*) only for the barrier region and (*b*) for the entire junction. Colour contour plots of these figures can be viewed at http//physics.nyu.edu/~pl2/.

has two paths of conduction when one uses the localized states, as well as the itinerant states in the electrodes.

These figures are plotted with a very small number (3600) of $\mathbf{k}_{\|}$ points that already show the difference between the two cases. Test calculations using 90 000 points in the whole 2D BZ show that the same conclusions still hold. From other convergence test calculations with both the number of $\mathbf{k}_{\|}$ points and with the number of nearest neighbours as mentioned earlier, we conclude that these differences are real and well above the numerical error range.

§6. Bias dependence of tunnelling currents and magnetoresistance

Based on the same technique we can push our effort one step further by introducing a finite voltage bias into these calculations. As in the previous calculations we calculate the resistance arising solely from the barrier and its interfaces with the electrodes. One of the major obstacles when making 'open circuit' transport calculations between two electrodes with different Fermi energies, that is for a tunnel junction that is not part of a closed circuit, is that self-consistency mandates that under an applied voltage there is a redistribution of electrons between electrodes so as to re-equilibrate the Fermi levels in both electrodes. However, what actually transpires in a junction that is part of a closed circuit and maintains a potential drop across it in the presence of a current is that the electron loss (gain) from an electrode is replenished (removed) by the wire completing the circuit. We are able to mimic the effects of voltage on the junction without undoing the difference in the electrode Fermi levels as follows. We first calculated the surface properties of a perfect ferromagnetic bcc Fe(100) surface in a constant external field; from this we calculate the JMR of a Fe/vacuum/Fe tunnel junction. The effect of a constant external field on the Fe/vacuum surface is simulated in SKKR either by shifting the work function or equivalently by adding a fixed layer of charge in the vacuum. By matching two Fe/vacuum surface systems calculated under equal but opposite external fields we obtain a Fe/vacuum/Fe MTJ under a voltage bias. In figure 9 we show the atomic potentials in the vacuum layers for Fe/vacuum(11)/Fe for zero bias and two applied biases that results from matching the two surface calculations. The

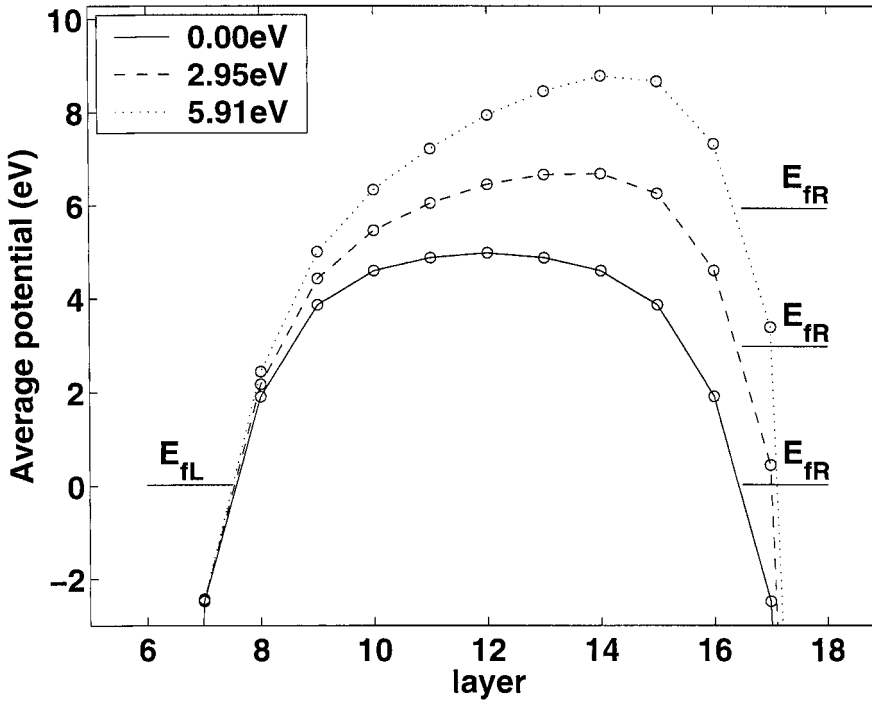

Figure 9. Average atomic potentials in all the vacuum barrier layers in a Fe/vacuum(11)/Fe tunnel junction resulted from matching two surface calculations. Values for three different voltage biases (0.00, 2.95 and 5.91 V) are plotted.

resulting potentials deviate from the trapezoidal barrier that is conventionally used; the negative potentials for the two vacuum layers adjacent to the Fe electrodes indicate that there is a finite density of electrons at the Fermi level for these layers. The density of states for majority and minority electrons at the surface of the Fe electrodes and one layer in from the surface are shown in figure 10. In the presence of a bias the DOS of one electrode has to be shifted relative to the other; in figure 11 we show these for parallel and antiparallel configurations of the electrode for the surface layers. The striking difference between zero and finite bias is the disparity between the DOSs of the same spin for the two electrodes *even when they are parallel.*

The tunnelling current densities and JMR of such a tunnel junction are then calculated using the same technique as for the linear response region. In figure 12 we show the spin-polarized tunnelling current density j for all four different combinations of the electrode spins as functions of the voltage bias. The notable difference from zero bias is the different current densities in the antiparallel configuration between the majority channel in the left-hand electrode and the minority channel in the right-hand electrode, and also between the minority channel in the left and the majority channel in the right; for zero bias they are identical. The channels with the minority spin on the right-hand side dominate the others. Current densities from channels with the majority-spin channel on the left-hand side (shown as open circles) present exponential-like behaviour in all the bias range, with virtually no fine structure, while those from channels with the minority spin channel on the left-hand side

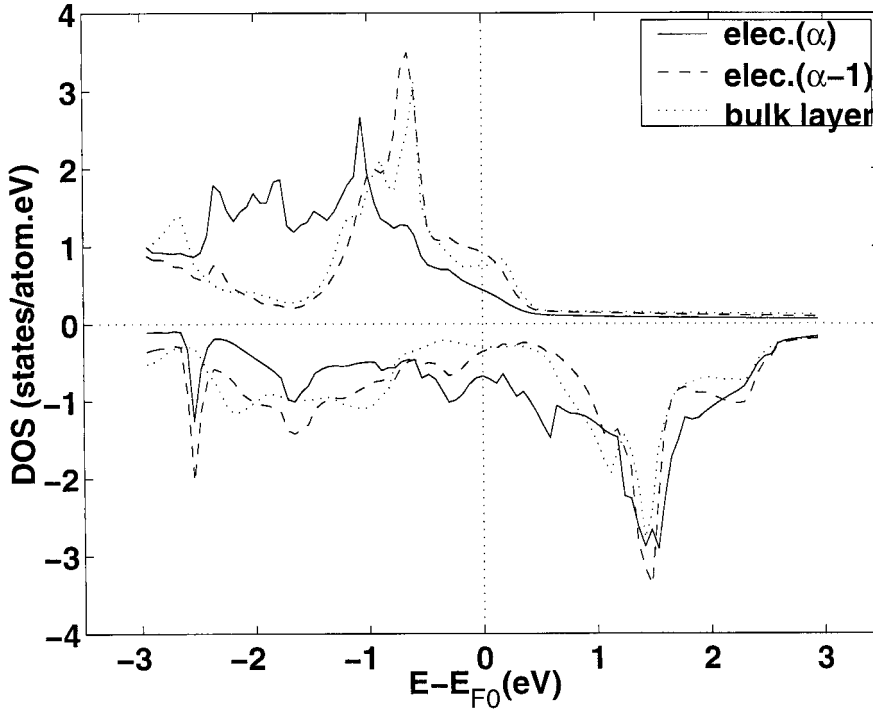

Figure 10. Spin-resolved DOSs around the Fermi level for the surface layer (elec.(α)) of the isolated electrode (——), the next-to-surface layer (elec.($\alpha - 1$)) layer of the electrode (– – –) and a bulk Fe layer (· · · · · ·). Positive values are for the majority spin channel and negative values are for the minority spin channel.

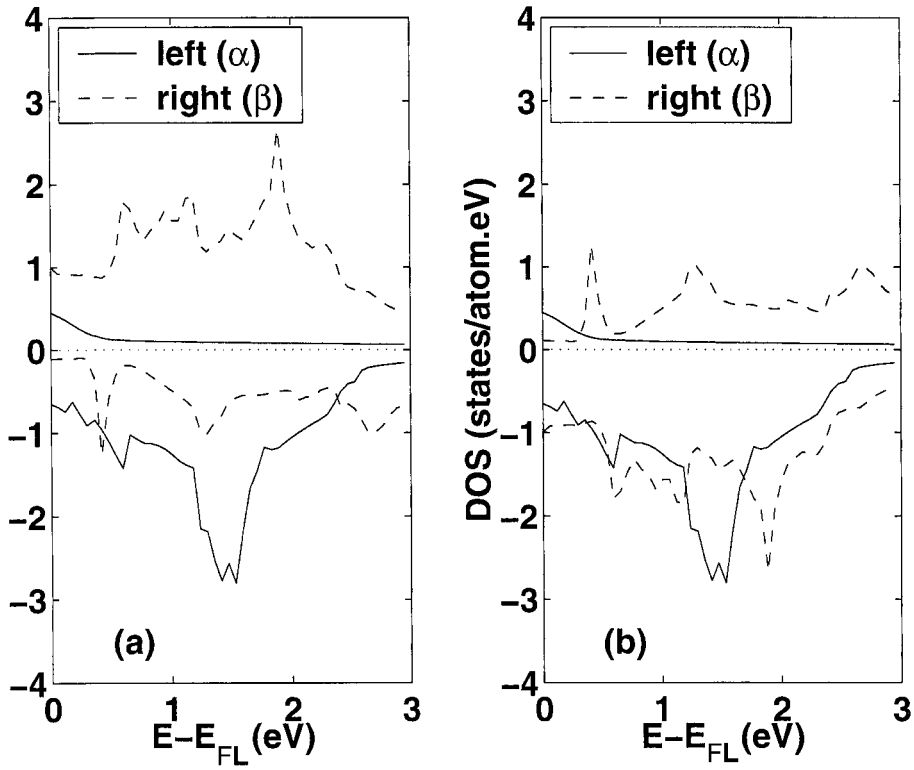

Figure 11. Spin-resolved DOSs around the left-hand electrode surface layer (layer α) and of the right-hand electrode surface layer (layer β) plotted at the same energy in a Fe/vacuum(11)/Fe tunnel junction under a voltage bias of 2.91 V for (*a*) the parallel configuration and (*b*) the antiparallel configuration. These plots are obtained from figure 10 by shifting the DOS of the right-hand electrode up by 2.91 eV.

(shown as crosses) demonstrate a little more intricate fine structure in the bias range from 0 to 1.5 V; they peak around a bias value of 0.3 V and then gradually decline and dip in the range 1.2–1.5 V. After that they also approach a behaviour reminiscent of tunnelling across a barrier with no features from the DOS. The exponential-like increases in the current densities are indicators that the bias is such that electrons at the Fermi level of the forward-biased electrode have a reduced barrier height and width.

From the current densities we calculated the JMR ratio as a function of the voltage bias. At zero bias, the JMR is 88%. This value drops to zero for approximately 0.6 V when the two dominating current density lines cross each other in figure 12 and continues to drop all the way down to −374% for a bias of about 1.5 V if we maintain the same definition of the JMR ratio (equation (7)). The aberrantly large negative value arises because the conductance of the parallel configuration becomes smaller than that for the antiparallel configuration when the ratio becomes negative and the denominator in the ratio is small. Therefore, to keep JMR ratios that are less than one, we use the larger conductance of the antiparallel configuration in the denominator of the JMR ratio when it is negative. In figure 13 we plot the JMR ratios for this revised definition of the negative JMR. After 1.5 V, as

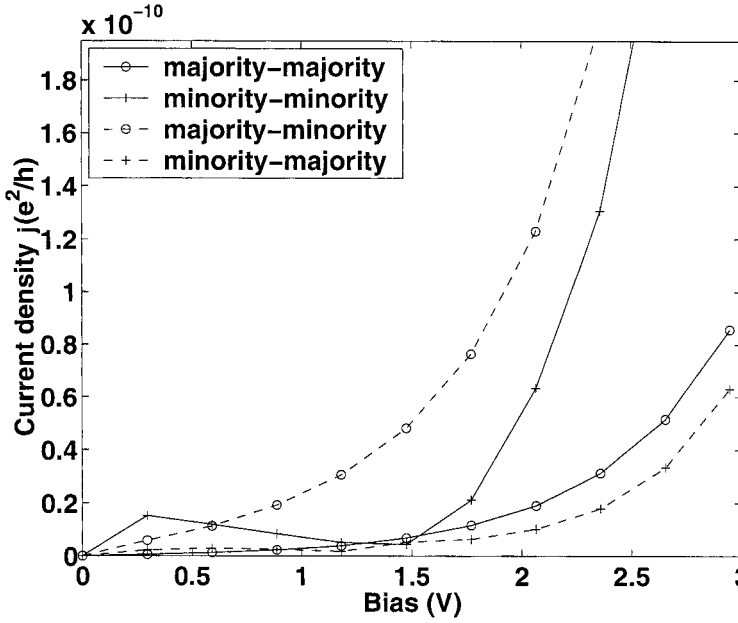

Figure 12. Spin-resolved tunnelling current density of Fe/vacuum(11)/Fe at different voltage biases for both the parallel configuration and the antiparallel configuration. The values for two of the curves at higher bias values are truncated to show the fine structure.

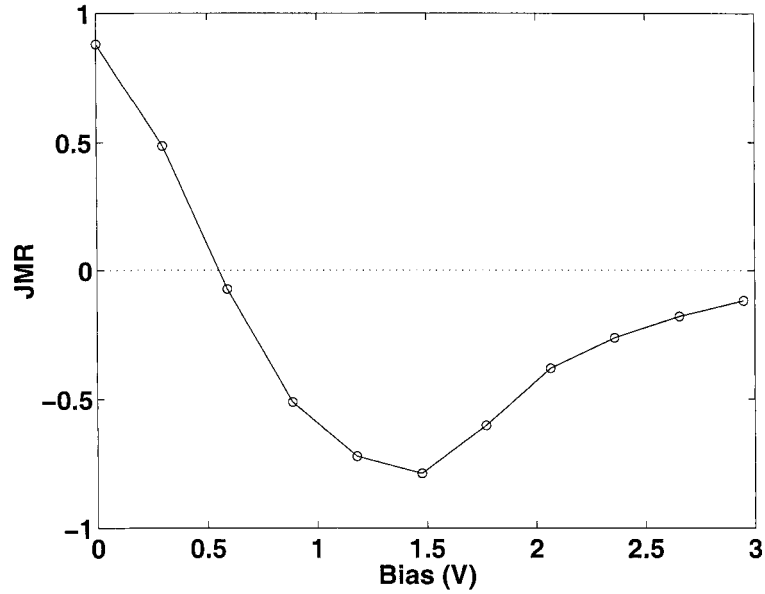

Figure 13. JMR ratio versus bias for a Fe/vacuum(11)/Fe tunnel junction according to the revised definition of the JMR in which the numerator is always the difference between parallel and antiparallel conductances but the denominator is the larger of these two values: (○), calculated values; (——), guide to the eye.

the exponential-like behaviour of the current densities set in, the JMR ratio quickly increases and approaches zero at higher biases.

To understand better which features of the bias dependence of the tunnelling current density and magnetoresistance depend on the details of the DOS of the electrodes and the potential profile of the barrier, we have made an exact calculation of the tunnelling current density by numerically solving the Schrödinger equation for a model of the junction with a trapezoidal barrier whose slope is given by the bias and in which the electrodes are represented by spin-split free-electron bands. In figures 14 and 15 we show the results for the tunnelling current densities and magnetoresistance. The parameters are chosen in such a way as to best reproduce the JMR curve in figure 13. While the magnitudes are quite different, the overall trend is captured by this simple model. By altering the relative depths of the majority and minority channels, one can considerably vary the magnitude of the JMR at zero bias and, by changing the barrier height, the bias dependence of the JMR. However, it is necessary to caution that the magnitudes of the JMR predicted by these model types of calculation are not reliable (Zhang and Levy 1998, 1999). Therefore, other than showing that the qualitative features of the bias dependence of the JMR can be broadly reproduced in a simple model of tunnelling in the presence of a bias, *ab initio* calculations such as those presented above are vital for a more accurate description of the non-equilibrium effects of voltage on tunnelling magnetoresistance.

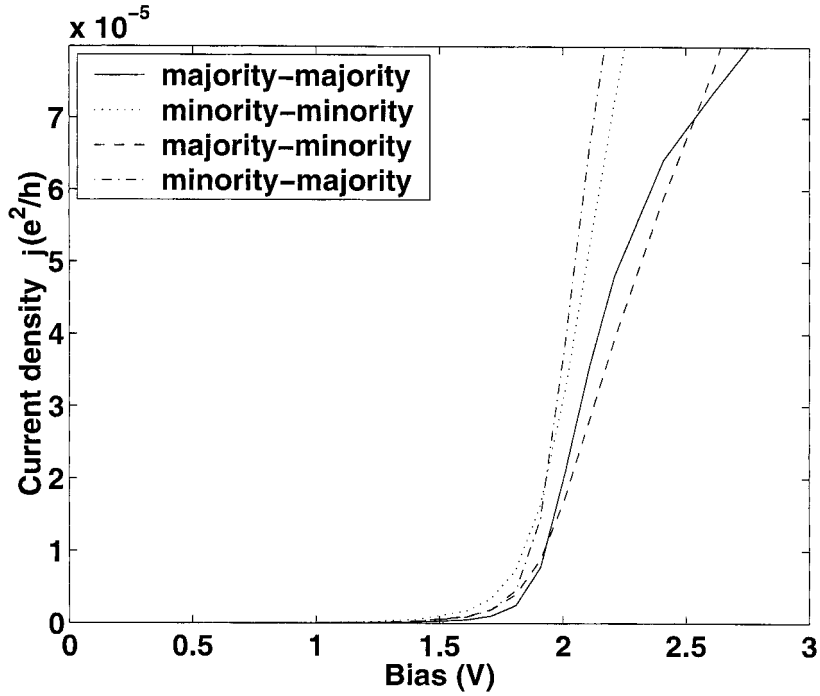

Figure 14. Spin-resolved tunnelling current density versus bias for a free-electron trapezoidal barrier model tunnel junction. The Fermi sea depth is 16 eV for the majority-spin channel and 3 eV for the minority-spin channel. The square barrier height at zero bias is 1 eV measured from the Fermi level.

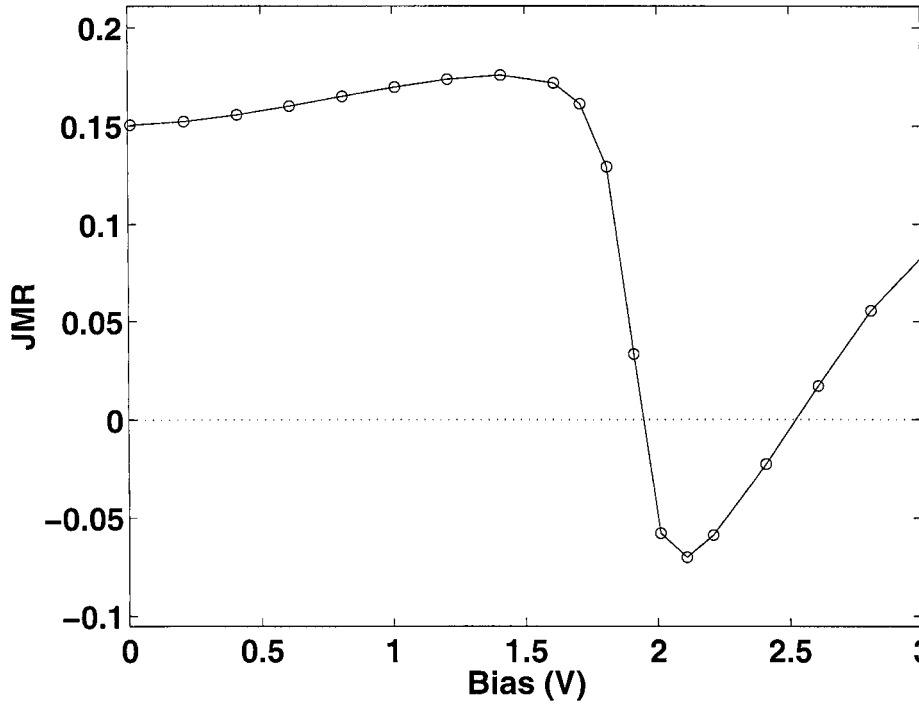

Figure 15. JMR ratio versus bias for the free-electron trapezoidal barrier model tunnel junction specified in figure 14: (○), calculated values; (——), guide to the eye.

§ 7. Summary

In tunnelling from one metal electrode through an insulating barrier into another metal electrode, the tunnelling properties depend on the electronic structures of the electrodes and barrier, as well as on the coupling between them. In theoretical discussions on tunnelling, it has been customary to make model calculations assuming that the hopping integrals are just constants, or taking them as free or fitting parameters, so as to show some aspects of tunnelling. In addition a square potential is usually assumed for the barrier profile. Both of these approximations lead to conclusions about the JMR of MTJs that are idiosyncratic (Zhang and Levy 1998, 1999). The *ab initio* calculations of the JMR for tunnel junctions to date have not included the putative roles of localized states at electrode–barrier interfaces in the conduction. To account in some measure for the influence on tunnelling of localized states at the electrode–barrier interfaces we have calculated the conductance across the barrier region alone; by placing reservoirs at the interfaces we are sure to fill these localized states. We undertook *ab initio* calculations of the JMR for tunnel junctions of bcc Fe(100), and for fcc Co(100) and fcc Ni(100) with various vacuum barrier thicknesses. The continuous Green's functions of the tunnel junction were obtained from *ab initio* band structure calculations using the SKKR method; the Green's functions entering the conductance formula were obtained by expanding them in a layer-resolved basis set for which the normalized scattering solutions from SKKR calculations were used. The isolated electrode Green's functions were derived from the coupled system Green's functions using Dyson's equation.

When the barrier thickness is small, the barrier region is strongly modified from a pure vacuum by electron hopping across the metal–barrier interface; in this range, the changes in the tunnelling conductance with barrier thickness are not exponential, and the JMR shows a dip at barrier thickness two to three atomic layers. When the barrier thickness is large, most of the barrier is just a constant potential and, as a result, the tunnelling conductance changes exponentially with the barrier thickness. For all barrier thicknesses in Co and Ni junctions, and for barriers thicker than two atomic layers in Fe junctions, negative spin polarization of tunnelling conductance was obtained; that is, the minority-spin channel dominates. This putatively agrees with some spin-polarized STM experimental results. Although there is no simple proportionality between the conductance and DOS of the electrodes, they do seem to be closely correlated, which suggests that the contribution of the d bands to tunnel across a vacuum is not small at all. This is in sharp contrast with tunnelling through alumina barriers where positive polarizations of tunnelling current was observed. It has been argued that, although the d band has a much larger DOS than the s band, because of its highly localized nature its contribution to tunnelling is negligible, that is, only the s band contributes significantly to tunnelling. Phrased differently, a part of the d electrons' energy is associated with its angular momentum; this in turn means that these electrons have lower kinetic energies. Our calculations indicate that the metal–barrier coupling plays an important role. Changes in tunnelling conductance and JMR with the thickness of the barrier are the results of the combined effect of the barrier band structure and the different couplings of the states at the electrode surface to the barrier. The bias dependence of the tunnelling currents in MTJs is controlled by the alteration of the potential barrier and by the shifts in the DOSs on the two sides of the barrier. The dip in the JMR at finite biases is reminiscent of that found in many studies.

Although we covered some aspects of magnetic tunnelling, our treatment is not applicable to conventional MTJs. Because of the limitations in our band structure calculation method, we have chosen vacuum as the tunnel barrier for its simpler structure. In reality, most experiments are made with insulators or semiconductors as barriers. These materials require band structure methods that can treat complex lattices. For simplicity, only perfect metal–barrier interfaces are considered in our calculations. While we based our calculation of the tunnelling conductance on all the states that exist at the electrode–barrier interfaces, it remains an open question as to the role of the interface roughness on the tunnelling properties and JMR of MTJs.

Acknowledgements

We thank Professor Peter Weinberger and Ingrid Mertig, Carsten Heide and Christoph Uiberacker for very fruitful discussions and their comments; we also thank Professor Supriyo Datta for several helpful discussions. This work was supported in its initial phase by the Office of Naval Research under grant N00014-96-1-0203, the National Science Foundation (grant INT-9602192) and NATO (grant CRG 960340). More recently this work was supported by the US Department of Defense Multidisciplinary University Research Initiative program administered by the Office of Naval Research under grant N00014-96-1-1207, and the Defense Advanced Research Projects Agency contracts MDA972-96-C-0014 and MDA972-99-C-0009.

NOTE ADDED SINCE SUBMISSION

Since we originally submitted this article a paper has appeared (Wunnich *et al.* 2002) which echoes some of our results, albeit through a different analysis. Indeed, it was Professor Dederichs who first opined that our results on tunnelling conduction could be due to the additional conduction channel through the localized states at the electrode–barrier interfaces.

APPENDIX A

Another method of evaluating the conductance is to start from equation (8) and to demand that all the Green's functions are expressed by unperturbed Green's functions of the isolated subsystems. We can use Dyson's equation $\mathbf{G} = \mathbf{g} + \mathbf{gVG} = \mathbf{g} + \mathbf{GVg}$, where $\mathbf{g}$ represents the Green's functions of the isolated subsystems, together with the *assumption of only nearest-neighbour hopping*, to find that

$$\begin{aligned} G^{ab} &= g^{ab} + g^{aa}V^{a\alpha}G^{\alpha b} + g^{ab}V^{b\beta}G^{\beta b}, \\ G^{\alpha b} &= g^{\alpha\alpha}V^{\alpha a}G^{ab}, \\ G^{\beta b} &= g^{\beta\beta}V^{\beta b}G^{bb}, \\ G^{bb} &= g^{bb} + g^{bb}V^{b\beta}G^{\beta b} + g^{ba}V^{a\alpha}G^{\alpha b}. \end{aligned} \tag{A 1}$$

Solving these equations for G^{ab} gives

$$G^{ab} = (1 - g^{aa}\Sigma^{aa})^{-1} g^{ab} (1 - \Sigma^{bb} g^{bb})^{-1}, \tag{A 2}$$

where $\Sigma^{aa} = V^{a\alpha} g^{\alpha\alpha} V^{\alpha a}$ and $\Sigma^{bb} = V^{b\beta} g^{\beta\beta} V^{\beta b}$ are self-energy terms on sites a and b respectively. As shown in equation (16), the hopping integrals are found by using the full Green's functions $\mathbf{G}$ and the unperturbed Green's functions $\mathbf{g}$.

We did not use this approach in our calculations for several reasons. Firstly, the explicit use of g^{ab} introduces more error because g^{ab} itself has to be derived from a suitably coupled system Green's function which again involves truncation in the coupling range; secondly, the extra manipulation of $\mathbf{V}$ reduces the numerical accuracy of the calculation; thirdly, because of the special way in which the energy band for a vacuum barrier is formed when coupled with a metal electrode, that is through charge redistribution, we found that this method was not able to reproduce satisfactorily the full Green's function G^{ab} as can be calculated directly in the present case. None the less, we mention it here for the following reasons.

(i) It is more amenable to theoretical analysis and model calculations than other formulations since in those analyses, more often than not, the unperturbed systems are, or are assumed to be, well known while the coupled system is totally unknown (for example Caroli *et al.* (1971)).
(ii) When we discuss the dependence of tunnelling on the external voltage across the barrier in terms of *ab initio* band structures, this may prove to be a very convenient, if not the only, method since to determine the bias dependence of tunnelling the conventional local density functional method cannot be applied to systems out of equilibrium.

In the current method, at least for thick barriers, we do not have to make a self-consistent calculation for the entire junction; a metal–insulator interface calculation

incorporating external field near the interface suffices and this has been shown to be quite feasible; see § 6.

While equation (18) holds for barriers thicker than one atomic layer, the special cases of barriers with one- or zero layer thickness are of some interest to us. When the barrier thickness is one atomic layer, then $a = b$:

$$t^{\beta\alpha} = V^{\beta a} G^{aa} V^{a\alpha}, \tag{A 3}$$

$$\begin{aligned} G^{aa} &= g^{aa} + g^{aa} V^{a\alpha} G^{\alpha a} + g^{aa} V^{a\beta} G^{\beta a} \\ &= g^{aa} + g^{aa} \Sigma^{aa} G^{aa} + g^{aa} \Sigma^{bb} G^{aa} \\ &= (1 - g^{aa} \Sigma^{aa} - g^{aa} \Sigma^{bb})^{-1} g^{aa}; \end{aligned}$$

so, roughly speaking, $(G^{aa})^{-1} \approx (g^{aa})^{-1} - \Sigma^{aa} - \Sigma^{bb}$, or $E \approx E^{aa} - \Sigma^{aa} - \Sigma^{bb}$, which explicitly shows the meanings of Σ^{aa} and Σ^{bb} as self energy terms.

When the barrier thickness is zero (i.e. $\alpha = a$ and $\beta = b$), the system is just bulk metal (for parallel alignment of the moments on both sides), and

$$G^{\alpha\beta} = g^{\alpha\alpha} V^{\alpha\beta} G^{\beta\beta}, \tag{A 4}$$

$$G^{\beta\beta} = g^{\beta\beta} + g^{\beta\beta} V^{\beta\alpha} G^{\alpha\beta}. \tag{A 5}$$

By solving for $G^{\alpha\beta}$ we find that

$$G^{\alpha\beta} = g^{\alpha\alpha} V^{\alpha\beta} (1 - g^{\beta\beta} V^{\beta\alpha} g^{\alpha\alpha} V^{\alpha\beta})^{-1} g^{\beta\beta}, \tag{A 6}$$

so that

$$\begin{aligned} t^{\beta\alpha} &= V^{\beta\alpha} + V^{\beta\alpha} G^{\alpha\beta} V^{\beta\alpha} \\ &= V^{\beta\alpha} [1 - g^{\alpha\alpha} V^{\alpha\beta} g^{\beta\beta} V^{\beta\alpha}]^{-1}. \end{aligned} \tag{A 7}$$

By placing this into the conductance equation (2), we rederive equation (7) of the paper by Mathon (1997) which was derived from the Kubo formula and used to calculate the ballistic conductance of bulk Co.

References

Alvarado, S. F., 1994, *New Trends in Magnetism Magnetic Materials and Their Applications,* edited by J. L. Morán-López and J. M. Sanchez (New York: Plenum), p. 175; 1995, *Phys. Rev. Lett.,* **75**, 513.

Alvarado F., and Renaud, P., 1992, *Phys. Rev. Lett.,* **68**, 1387.

Bode, M., Getzlaff, M., and Weisendanger, R., 1998, *Phys. Rev. Lett.,* **81**, 4256; 1999, *J. vac. Sci. Technol.* A., **17**, 2228.

Butler, W. H., Zhang, X.-G., Wang, X., van Ek, J., and MacLaren, J. M., 1997, *J. appl. Phys.,* **81**, 5518; 2001, *Phys. Rev.* B, **63**, 054416.

Butler, W. H., Zhang, X.-G., Schulthess, T. C., and MacLaren, J. M., 2001, *Phys. Rev.* B, **63**, 092 402.

Büttiker, M., 1988, *IBM J. Res. Dev.,* **32**, 317.

Caroli, C., Combescot, R., Nozieres, P., and Saint-James, D., 1971, *J. Phys.* C, **4**, 916; 1972, *ibid.,* **5**, 21.

Combescot, R., 1971, *J. Phys.* C, **4**, 2611.

Datta, S., 1995, *Electronic Transport in Mesoscopic Systems* (Cambridge University Press), pp. 161–163.

De Teresa, J. M., Barthélémy, A., Fert, A., Contour, J. P., Lyonnet, R., Montaigne, F., Seneor, P., and Vaurès, A., 1999a, *Phys. Rev. Lett.,* **82**, 4288; 1999b, *Science,* **286**, 507.

DUKE, C. B., 1969, *Tunneling in Solids* (New York: Academic Press).
GUNNARSSON, O., and LUNDQVIST, B. I., 1976, *Phys. Rev.* B, **13**, 4274.
INOUE, J., and MAEKAWA, S., 1996, *Phys. Rev.* B, **35**, R11 927.
JULLIERE, M., 1975, *Phys. Lett.* A, **54**, 255.
KRANS, J. M., and VAN RUITENBEEK, J. M., 2002, Preprint.
LANDAUER, R., 1988, *IBM J. Res. Dev.,* **32**, 306.
LEVY, P. M., WANG, K., DEDERICHS, P. H., CARSTEN, H., ZHANG, S., SZUNYOGH, L., and WEINBERGER, P., 2002, *Phil. Mag.* B, **82**, 763.
MACLAREN, J. M., ZHANG, X.-G., and BUTLER, W. H., 1997, *Phys. Rev.* B, **56**, 11 827.
MACLAREN, J. M., ZHANG, X.-G. BUTLER, W. H., and WANG, X., 1999, *Phys. Rev.* B, **59**, 5470.
MAEKAWA, S., and GÄFVERT, U., 1987, *IEEE Trans. Magn.,* **18**, 707.
MATHON, J., 1997, *Phys. Rev.* B, **56**, 11 810.
MATHON, J., and UMERSKI, A., 2001, *Phys. Rev.* B, **63**, 220 403(R).
MATHON, J., UMERSKI, A., and VILLERET, M. A., 1997, *Phys. Rev.* B, **55**, 14 378.
MESERVEY, R., and TEDROW, P. W., 1994, *Phys. Rep.,* **238**, 173.
NGUYEN-MANH, D., YU. TSYMBAL, E., PETTIFOR, D. G., ARCANGELI, C., TANK, R., ANDERSEN, O. K., and PASTUREL, A., 1998, *Mater. Res. Soc. Symp. Proc.,* **492**, 319.
OLEINIK, I. I., YU. TSYMBAL, E., and PETTIFOR, D. G., 2000, *Phys. Rev.* B, **62**, 3952.
PAPANIKOLAOU, N., NONAS, B., HEINZE, S., ZELLER, R., and DEDERICHS, P. H., 2000, *Phys. Rev.* B, **62**, 11 118.
PENDRY, J.B., PRETRE, A. B., and KRUTZEN, B. C. H., 1991, *J. Phys.: condens. Matter,* **3**, 4313.
POLLMANN, J., and PANTELIDES, S. T., 1978, *Phys. Rev.* B, **18**, 5524.
SZUNYOGH, L., ÚJFALUSSY, B., WEINBERGER, P., and KOLLÁR, J., 1994, *Phys. Rev.* B, **49**, 2721.
TODOROV, T. N., 1996, *Phys. Rev.* B, **54**, 5801.
TODOROV, T. N., BRIGGS, G. A. D., and SUTTON, A. P., 1993, *J. Phys.: condens. Matter,* **5**, 2389.
YU. TSYMBAL, E., OLEINIK, I. I., and PETTIFOR, D. G., 2000, *J. appl. Phys.,* **87**, 5230.
YU. TSYMBAL, E., and PETTIFOR, D. G., 1997, *J. Phys.: condens. Matter,* **9**, L411.
WANG, K., 1999, PhD Dissertation, New York University, New York, USA.
WEINBERGER, P., 1990, *Electron Scattering Theory for Ordered and Disordered Matter* (Oxford: Clarendon).
WEINBERGER, P., SZUNYOGH, L., BLAAS, C., and SOMMERS, C., 2001, *Phys. Rev.* B, **64**, 184 429.
WORTMANN, D., HEINZE, S., KURZ, PH, BIHLMAYER G., and BLUGEL, S., 2001, *Phys. Rev. Lett.,* **86**, 4132.
WUNNICKE, O., PAPANIKOLAOU, N., ZELLER, R., DEDERICHS, P. H., DRCHAL, V., and KUDRNOVSKÝ, J., 2002, *Phys. Rev.* B, **65**, 064 425.
ZHANG, S., and LEVY, P. M., 1998, *Phys. Rev. Lett.,* **81**, 5660; 1999, *Eur. Phys. J.* B, **10**, 599.